Design and Performance Improvement of Radial Line Slot Array Antennas

By

Mst. Nishat Yasmin Koli

A thesis submitted to Macquarie University

for the degree of Master of Research

Department of Engineering

24 April 2017

MACQUARIE
University
SYDNEY·AUSTRALIA

Typeset in LaTeX 2_ε.

The work presented in this thesis was carried out at the Department of Engineering, Macquarie University, Sydney, Australia, between July 2016 and April 2017. This work was principally supervised by Professor Karu Esselle and the co-supervision was done by Dr Raheel Maqsood Hashmi. Except where acknowledged in the customary manner, the material presented in this thesis is, to the best of my knowledge, original and has not been submitted in whole or part for a degree in any other university or institution other than Macquarie University.

Nishat Yasmin

_____

Mst. Nishat Yasmin Koli

Abstract

Rapid increase in satellite-based wireless services has created a demand for directive beam-steering antennas with wide radiation bandwidths. Commercially available parabolic reflectors provide satisfactory performance but their bulky physical appearance and nonplanar configuration make them less attractive in several applications. Microstrip array antennas exhibit poor radiation efficiency at higher gain. Radial line slot array (RLSA) antennas are known for their directive radiation characteristics and planar profile but suffer from limited radiation bandwidth and lack the beam-steering feature. This thesis presents RLSA antennas with improved radiation performance, wide radiation bandwidth and beam-steering feature. Several RLSA antennas have been designed. One of these RLSA antennas has a gain of 36.9 dBic with radiation efficiency greater than 90%. By optimising near-field amplitude distribution, sidelobe level of an RLSA antenna has been reduced to -26.1 dB, which comes close to Class-2 and Class-3 ETSI antenna standards. RLSA radiation bandwidth has been enhanced by introducing permittivity variation of the dielectric materials in the cavity. Such an antenna has demonstrated a 3-dB directivity bandwidth of 19.4% and an axial ratio bandwidth of 27.3%. Furthermore, this thesis also presents a methodology to steer the beam of RLSA antennas by using a pair of near-field phase-transforming metasurfaces.

Acknowledgments

List of Publications

- **Nishat Y. Koli**, Muhammad U. Afzal, Karu P. Esselle and Raheel M. Hashmi, *"Compromise Between Bandwidth and Pattern Quality in Circularly Polarized Radial Line Slot Array Antennas*," Fifteenth Australian Symposium on Antennas (ASA), Sydney, Australia, 7-8 Feb. 2017.

Contents

List of Figures

List of Tables

Chapter 1

Introduction

The upcoming smart communication system of future wireless technologies requires antennas to meet stringent standards and possess a range of capabilities. For any communication system, it is highly desirable to have an antenna with adequate gain, large bandwidth, stable radiation pattern, and beam reconfigurability. This is particularly true for satellite-based wireless services envisaged in the near future, which will require highly directional antennas.

Parabolic reflector antennas have been utilised for several years in terrestrial and satellite communication systems. These antennas perform well in terms of gain, coverage, and radiation efficiency. However, while they are relatively inexpensive, they occupy a large physical volume which makes them undesirable for several applications such as satcom-on-board-aircraft and satellite-on-the-move. Furthermore, their nonplanar format makes a difficulty for manufacturing, transportation, and deployment. In order to address these practical limitations, a significant attempt has been made to find alternatives to parabolic reflector antennas with a low weight, low profile, and more aesthetic appeal, while achieving comparable performance metrics. Microstrip patch array antennas are popular for their high gain and planar surface, but the complex feed network limits the antenna performance significantly.

Therefore, the demand for more aesthetically pleasing antennas creates an opportunity to search for a suitable alternative to the parabolic reflector and microstrip patch array antennas. It is apparent that a mid-way solution is desired to provide high-gain, efficient characteristics like a parabolic reflector while adhering to the low-profile, planar design of patch array, but without a bulky structure and complex feed network. Radial line slot array (RLSA) antennas have shown the capability to meet these stringent requirements. The main advantage of RLSA antennas is that high gain, low profile, and good antenna efficiency can be achieved with only a single feed structure while adhering to a planar,

simple parallel-plate radial waveguide-like-structure.

1.1   Motivation of the Research

Currently, for long-distance communication, high-frequency and high-gain antennas with standardised radiation patterns are highly desirable to transmit or receive signals. These antennas are the key components in direct broadcasting systems, satellite communication, backhaul networks, point-to-point communication, high power microwave (HPM) applications, etc. The growing demand for beam-steering techniques compatible with these antennas is extremely desirable for satellite reception, space exploration, wireless local-area networks (WLAN) as well as in cellular communication. RLSA antennas are considered to be the most attractive and versatile candidate for these applications because of their promising features (high gain, low profile) and historically proven successful application. Their compactness and high efficiency are also applicable for other applications such as medical imaging, radiometry, and near-field probing. The RLSA antenna is deemed to be a potential candidate to serve as an alternative to traditional high-gain antennas and beam-steering applications. Despite several benefits, the factor that limits RLSA antennas in some applications is their narrow radiation bandwidth. This provides the motivation to increase the bandwidth of RLSA antennas and investigate their potential to satisfy the various requirements.

1.2   Research Framework and Objectives

The research presented in this thesis has been conducted over a period of nine months beginning in July 2016, for partial fulfilment of the requirements for the degree of Master of Research (MRes) in Macquarie University. The research was funded by an international Research Training Pathway (iRTP) scholarship. Based on Macquarie University MRes thesis guidelines, the main body of the thesis is restricted to a maximum of 55 pages, approximately.

The first objective of this thesis is to improve the radiation performance and pattern quality of RLSA antennas by optimising the field distribution. The second objective is to enhance the limited radiation bandwidth of RLSA antennas. The third objective is to steer the radiation beam of RLSA antennas to meet the growing demands of several wireless applications.

1.3 Thesis Organisation and Contributions

The thesis is organised into seven chapters including a brief introduction in Chapter 1 and the concluding remarks documented in Chapter 7. The remaining 5 chapters are arranged as follows:

Chapter 2 provides a generalised overview and background of RLSA antennas. A literature review of the development of RLSA antennas is presented. Some cutting-edge applications of RLSA antennas in different communication areas are also described in this chapter.

Chapter 3 presents the basics of the RLSA antenna design process and explains the key terminologies being used throughout the thesis. A theoretical explanation on producing the correct polarisation is given. The main contribution of this chapter is an optimised design methodology to model single-layer circularly polarised (CP-RLSA) antennas. This model simplifies the design and analysis procedures of RLSA antennas. A CP-RLSA antenna has been designed using this procedure and has demonstrated a peak gain of 36.9 dBic with 95% antenna efficiency. A significant improvement has been made in the sidelobe levels with an appropriate radiation pattern envelope (RPE) values.

Chapter 4 presents an investigation of the aperture illumination of RLSA antennas. For this purpose, two CP-RLSA antennas have been designed with different layouts of slot radiators, to achieve uniform and tapered amplitude distributions on the aperture. The distributions were optimised by controlling the slot coupling. Numerical results of these two aperture distributions are presented and compared. The uniform distribution demonstrates a high gain with large gain bandwidth whereas the tapered distribution provides a broadside beam with controlled sidelobe levels.

Chapter 5 presents the methodology to enhance the radiation bandwidth of RLSA antennas. A new design configuration of the RLSA antenna cavity is proposed to improve the radiation bandwidth. The cavity was designed with radial permittivity variation of the dielectric materials in the transverse direction. Numerical results predicted an increase in 3-dB directivity and gain bandwidth up to 19.4% with a peak directivity of 32.5 dBi. A good impedance matching has been observed within the operating frequency band. Additionally, the antennas have revealed their ability to satisfy ETSI Class-2 and Class-3 antenna RPEs.

Chapter 6 presents a beam-steering method for RLSA antennas. The method requires a pair of phase-transforming metasurfaces in the near-field region of the RLSA antenna. These metasurfaces are then physically rotated to move the beam over a large conical region. A prototype has been designed and simulated to steer the beam in a conical region with a vertex angle of 84° .

Chapter 2

Background

2.1 Radial Line Slot Array (RLSA) Antennas

The radial line slot array (RLSA) antenna is a slotted-waveguide planar antenna. It consists of a circular aperture with a radial waveguide which supports the transverse electromagnetic (TEM) travelling-wave mode. The typical configuration of an RLSA antenna is illustrated in Figure 2.1. The antenna is composed of two parallel conducting plates with a distance (d) apart. The top plate consists of radiating slot patterns and the bottom plate acts as a ground plane. Slots are used to couple with the radial currents flowing through the aperture.

The radial waveguide formed between these two plates is filled with a dielectric material of relative permittivity $(\varepsilon_r) > 1$. This dielectric material helps to reduce the slot spacing, by the factor $\sqrt{\varepsilon_r}$, to be smaller than the free-space wavelength. This benefits the waveguide by creating a slow wave structure within the guided wavelength (λ_g) to avoid grating lobes in the radiation patterns. The dielectric materials in an RLSA antenna should have relatively low losses, be isotropic, and have a reasonable effective permittivity. The power is fed to the antenna via a single coaxial probe embedded in the centre, between the upper and lower plates.

The RLSA antenna can operate either in transmit mode or in receive mode. Based on the slot design configuration, RLSA antennas are categorised as linearly polarised (LP) or circularly polarised (CP). The desired polarisation can be achieved by appropriately selecting the layout and orientation of the slots on the upper plate. In an LP-RLSA antenna, the slot sets are spaced by half guided wavelength, which produce large reflections at the centre point. In CP-RLSA antennas, the slot sets are spaced by a quarter guided wavelength, producing smaller reflections at the centre point. Therefore, a CP-RLSA antenna provides a higher return loss than an LP-RLSA antenna. Reflection-cancelling slots and beam

tilting techniques are used to improve the return loss in the LP-RLSA antenna.
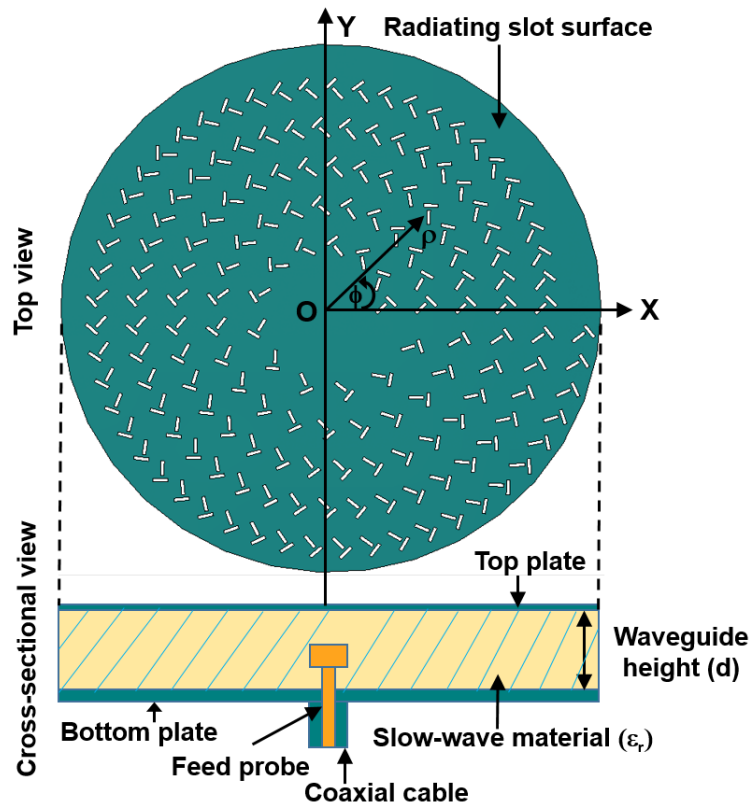
Figure 2.1: Top and side view of a single-layer RLSA antenna. The antenna has two metallic plates; the top plate has radiating slots and the bottom plate acts as a ground plane. The antenna is fed by a coaxial cable from the bottom.

2.2   Development of RLSA Antenna Technology

RLSA antennas emerged from the slotted waveguide array family, which is a very promising technology for high-gain antennas. RLSA antennas were first introduced by Kelly in the early 1960s [7, 8]. The antennas were made of annular rings of crossed slots and fed from a complicated feeding structure. This concept was modified by Ando and Goto [5, 9]. They proposed an alternative slot arrangement in the form of a spiral array. It was made of a double layered cavity and provided circular polarisation. The feeding complexity was removed by the proposed antenna, but the double-layered cavity created several difficulties for manufacturing. Takahashi developed a single-layered cavity of RLSAs which removed the limitations brought by the double-layered cavity [10]. A slot configuration for linearly polarised RLSA antenna was proposed in [11]. The reflections from slots were higher in the LP-RLSA

antenna than for the CP-RLSA antenna. The cross-polarisation components were greater than the co-polarisation components which degraded the antenna's performance.

A slot arrangement for reflection cancellation in the LP-RLSA antenna was proposed and return loss was improved [12]. A dual circularly polarised RLSA antenna was designed for the application of direct broadcast from satellite (DBS) reception [13]. The author presented a new type of radial line slot array antenna which is a combination of the single and double-layered cavity for wider bandwidth. A dual circularly polarised RLSA antenna was investigated [14]. The author introduced the feasibility and optimised the slot design of the CP-RLSA antenna. A double pin coaxial adapter served to excite the travelling waves in the cavity. The antenna gain of 33.5 dBic and efficiency 70% were measured with 0.55-meter diameter antenna. Based on the earlier study, Paul Davis developed the design methodology for LP-RLSA antenna [15–18]. The antenna efficiencies were measured as 67% for 600 mm and 58% for 400 mm diameter antennas [15]. By incorporating reflection cancelling slots, return loss of the antenna (S_{11}) was improved from -5 to -20 dB with a directivity of 35 dBi. A CP-RLSA antenna was designed with slots arranged in a concentric array for monopulse application as illustrated in Figure 2.2 [1]. Two beams were obtained: one was a boresight beam with a constant phase in azimuth angle, and the other was a conical beam whose phase was dependent on azimuth angle.

For the application of wireless local area networks (WLAN), a low-cost CP-RLSA antenna was proposed [19]. The RLSA antenna was used as an alternative of microstrip patch and wire monopole antennas. A slot coupling analysis utilising the method of moments (MoM) with double layer dielectrics was presented in [20]. The layers are made of PTFE and foam materials. Two models were investigated, and 35.5 dBi directivity with efficiency 70-80% were achieved in both models. An LP-RLSA antenna prototype was constructed [21]. Reflection cancelling and beam-squinted techniques were employed to improve the S-parameter. An antenna gain of 33 dBi was achieved with a return loss
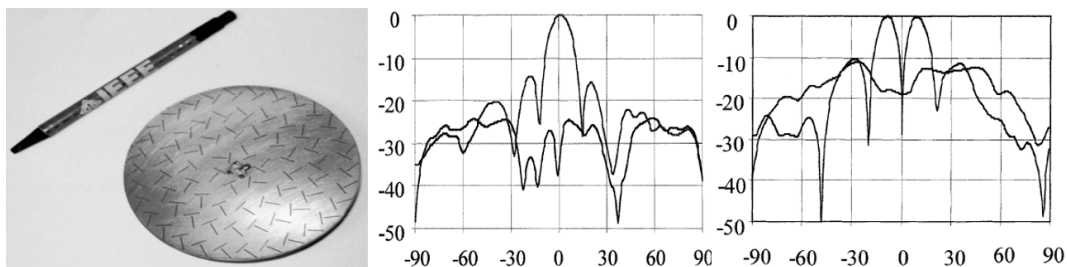
Figure 2.2: (left) Fabricated prototype of CP-RLSA antenna, (middle) Radiation pattern-pencil beam at 13.7 GHz, (right) Radiation pattern-conical beam at 13.7 GHz [1].
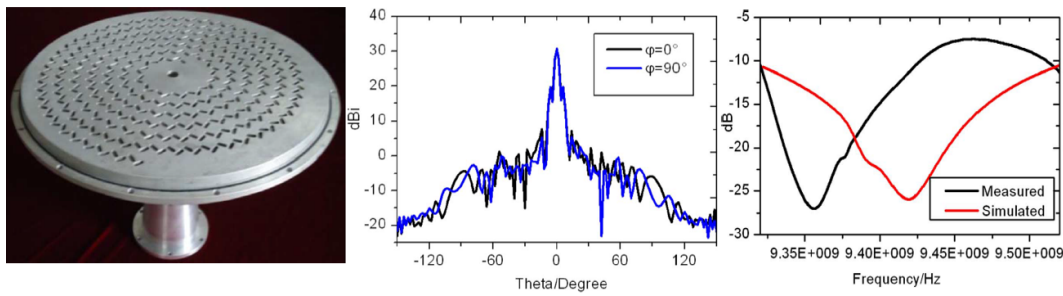
Figure 2.3: (left) Fabricated HPM-RLSA antenna, (middle) Directivity pattern at 9.42 GHz, (right) Measured and simulated reflectance coefficient [2].

greater than -21 dB. An automatic design of CP-RLSA antenna was presented with three examples as follows: firstly, pencil beam with the highest directivity; secondly, a boresight beam with lower sidelobes; and thirdly, a shaped beam isoflux radiation pattern [22].

In 2013, a radial-line slow-wave structure was designed to replace the traditional dielectric sheet for high power microwave (HPM) application as given in Figure 2.3 [2]. The antenna has shown a power handling capacity of 1 GW. The aperture efficiency was measured as being 44.8% at 9.42 GHz, gain 29.0 dBi and the axial ratio of 1.6 dB. One limitation with this design is that the efficiency degraded due to rotational asymmetry of illumination. In 2015, a concentric array (CA) RLSA antenna design method was proposed to overcome this problem [23]. The design achieved a gain of 32.0 dBi, an axial ratio of 0.5 dB and an aperture efficiency of 62.7% at 12 GHz. An RLSA antenna was presented to compare the Ka-band and Ku-band DBS receiver in terms of bandwidth availability, and directivity [24]. To reduce the sidelobe level and improve the impedance bandwidth, an antenna was designed for mobile broadband application [25]. A gain of 23.3 dB and sidelobes level of -16.5 dB were realised. A CP-RLSA antenna was presented for the frequency offset [26]. A gain of 30.8 dBi at 11.8 GHz was achieved with a simulation carried out by Matlab and HFSS interface technology. The author has investigated the effect of the slots without and with dielectric structure (FR4) in [27]. Slots without dielectric structure performed a better bandwidth (44%) and return loss (-24 dB) compared to the slots with a dielectric structure.

Many prototypical RLSA antennas were manufactured with honeycomb structures for satellite on-board applications [3, 28–30]. Good antenna performances were achieved with a gain of 44.6 dB at 32 GHz for a 90 cm RLSA antenna and the weight was only 1 kg due to the honeycomb structure as shown in Figure 2.4 [3]. A difficulty associated with this design is the large loss factor (0.014 0.018 dB/mm)
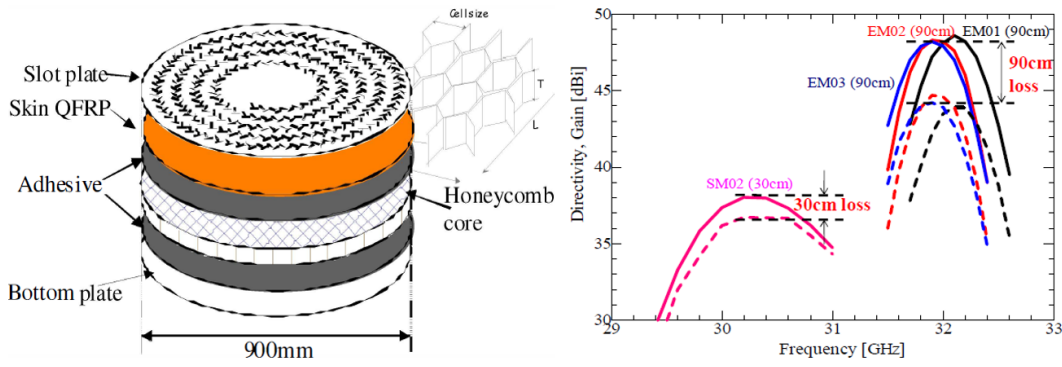
Figure 2.4: (left) RLSA with multilayered waveguide including honeycomb structure, (right) Measured antenna performances of the fabricated prototypes with estimated losses [3].

which degrades the antenna performances. To achieve high gain and lower side lobe levels, a single layered CP-RLSA was designed, filling the cavity with foaming material [31]. Modifying the angle and varying the slot length, the gain was obtained. An RLSA antenna with dipole polariser was utilised to metamorphose the circular polarisation to linear polarisation [32]. Since the reflection cancelling method makes the antenna structure more complicated, the author placed the polariser as double layer dipole arrays over the CP-RLSA. Sidelobe level of -21.7 dB, directivity 31.5 dB and antenna efficiency of 65% were achieved for the 250 mm diameter antenna. A parasitic dipole was used to minimise reflections as well as to improve matching in LP-RLSA antenna [33]. Different types of feed structure design mechanisms of RLSA antennas were presented and analysed to match the impedance of the waveguide [34, 35]. A new slot layout of dual spirally arranged RLSA antenna was presented in [36]. The return loss improved from -15 dB to -30 dB compared to reflection cancelling and beam-tilted designs. To optimise the RLSA weight, two lightweight planar CP-RLSA antennas were presented, one for reception and another one for transmission [37]. Two-layered dielectric substrates were used to minimise the antenna weight. Radiation efficiency of 70%, and directivity of 27 dBi were achieved with 400 mm diameter antenna.

2.3   Applications of RLSA Antennas

RLSA antennas have attracted significant attention from the research community because of their high gain, low profile, and simple configuration, which is in contrast to other traditional planar antennas. The antennas are often used in the microwave and millimetre wave bands. The planar surface of an RLSA antenna helps it to retain immunity to leaf, water or snow build-up. The conductor and dielectric materials make the body of RLSA antennas hard and robust. An RLSA antenna can

easily be mounted on a wall or roof because of its low profile and ease of installation. The cost of manufacturing for an RLSA antenna is also very low. High efficiency and a pleasant aesthetic appearance make the RLSA antenna an attractive candidate for point-to-point communications, point-to-multipoint communications, and direct broadcast from satellite reception [4, 5, 9, 15, 16]. RLSA antennas are also very popular for high-power microwave applications, and high-density plasma etching [2, 6, 23]. The low-cost feature of RLSA antennas is suitable for wireless local-area network (WLAN) applications and space solar power system [6, 19]. Nowadays, RLSA antennas are being increasingly used in space exploration and satellite communications [3, 28, 29, 37]. Some RLSA antenna applications in different communication areas are shown in Figure 2.5.

Direct broadcast from satellite (DBS) reception

High-power microwave application

Conical-beam RLSA antenna for satellite on the move DBS receiver

RLSA antenna with honeycomb structure for space exploration

Millimetre-wave application

Plasma etching with RLSA antenna
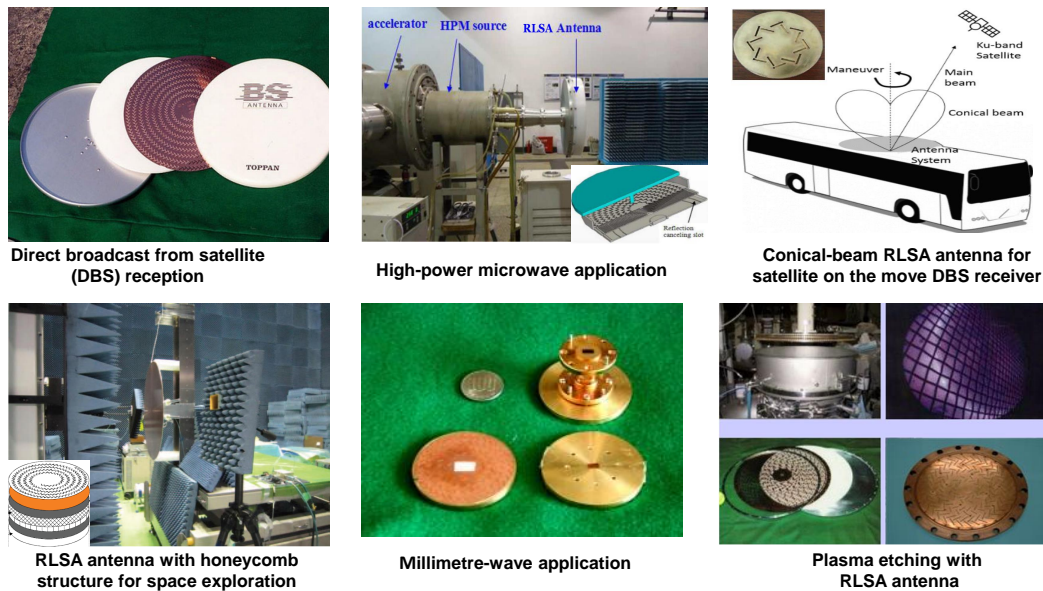
Figure 2.5: Application of RLSA antennas in different areas [2–6].

2.4   Radiation Bandwidth of RLSA Antennas

Recent literature suggests several promising techniques to overcome the limitations of RLSA antennas associated with gain, return loss, and efficiency. However, the main limitation of RLSA antennas is associated with the narrow radiation bandwidth. The directivity bandwidth decreases as the gain increases. This limits their utilisation in several applications where high gain and wider radiation bandwidth are desired.

Chapter 3

Radial Line Slot Array Antenna Design Methodology

3.1   Introduction

A generalised overview of RLSA antennas has been presented in Chapter 2. This chapter presents a method for designing a classical RLSA. It is worth noting here that our emphasis in this chapter is on a single-layer circularly polarised (CP) RLSA antenna due to its simplicity and application in long-range satellite communication. The main contribution of this chapter is a simplified design and analysis procedure of RLSA antenna which is explained with an example.

Before explaining the design process, an important aspect of RLSA antenna design is to determine what general conditions are required for circular or linear polarisation. For this reason, a brief theoretical explanation on selecting the correct polarisation is presented in Section 3.2. Section 3.3 describes the operational principle and an in-depth analysis of RLSA antennas along with modelling a design example. To verify the antenna performances, full-wave simulation results are illustrated in Section 3.4.

3.2   Polarisation in RLSA Antennas

The polarisation of an antenna depends on the characteristics of the radiated waves. The relationship of field polarisation with RLSA antenna geometry is explained here with an example. If a plane wave in free space is travelling in the $\hat{z}$ direction, the two orthogonal field components of the wave can be

written as [38]:

$$\tilde{E}(z,t) = E_x(z,t)\hat{x} + E_y(z,t)\hat{y} \tag{3.1}$$

The instantaneous expressions of the field components are:

$$E_x = A_x cos(\omega t - kz + \phi_x) \tag{3.2}$$

$$E_y = A_y cos(\omega t - kz + \phi_y) \tag{3.3}$$

where A_x and A_y are the magnitudes of the x and y components, respectively. For the wave to have linear polarisation, the phase difference between the two orthogonal field components must be an integer multiple of π. That is:

$$\triangle\phi = \phi_x - \phi_y = n\pi, n = 0, 1, 2, 3... \tag{3.4}$$

Circular polarisation is achieved only when the magnitudes of the two field components are identical and the phase difference between them is an odd multiple of $\pi/2$. Algebraically the requirements can be written as:

$$|E_x| = |E_y| \Rightarrow A_x = A_y \tag{3.5}$$

$$\triangle\phi = \phi_x - \phi_y = \begin{cases} \pi/2 + n\pi, & \text{n=0,1,2... for CW} \\ -\pi/2 - n\pi, & \text{n=0,1,2... for CCW} \end{cases} \tag{3.6}$$

where CW designates a clockwise rotating electric field vector and right-hand circular polarisation, and CCW designates a counter-clockwise rotating field vector and left-hand circular polarisation. When designing RLSA antennas, the two field components are generated by a slot pair. This slot pair must radiate the field components with correct phase and amplitude depending on the desired polarisation. Additionally, the components must have a proper orientation. The slots' orientation is a critical design step that must meet the required specifications. A slot geometry for creating a right-hand circularly polarised RLSA antenna is discussed in the following section.

3.3 Design Steps

The design process of a CP-RLSA antenna can be divided into three steps as summarised in the flow chart in Figure 3.1. The design is explained using Figure 2.1 as a reference. The first step in the design process is to create the layout of slots on the top plate of the antenna. The slot configuration here

is made using Visual Basic (VBA) macros in CST Microwave Studio. The second step is to design the radial waveguide which supports the outward travelling waves within the cavity while the third step includes feed-transition design in order to feed the antenna. A detailed explanation of this design process is given in the following subsections.
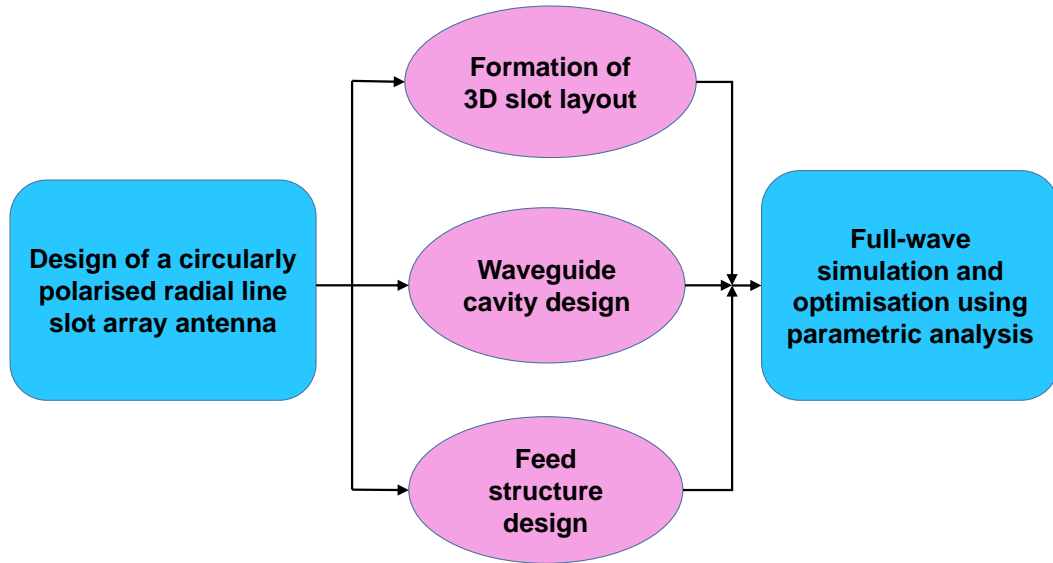
Figure 3.1: Flow chart summarising the CP-RLSA antenna design process.

3.3.1   Slot Configuration

The slot surface design includes determining the location and orientation of all slots. The arrangement of slots is also a two-step process, in which:

- Step one is to design a unit radiator consisting of two orthogonal slots. This slot-pair fulfils the CP condition as explained in the previous section.

- Step two is to arrange these slot pairs on the entire top surface. These pairs are arranged such that the field radiated by each pair adds constructively towards the broadside direction.

The slot geometry of a unit radiator is given in Figure 3.2, with two adjacent slots (slot~1 and slot~2) lying along the ϕ direction. The two slots are situated orthogonally to radiate orthogonal field components. Critical parameters associated with the slot pair are summarised below.

ρ_1 : distance from the origin O to the centre of slot~1
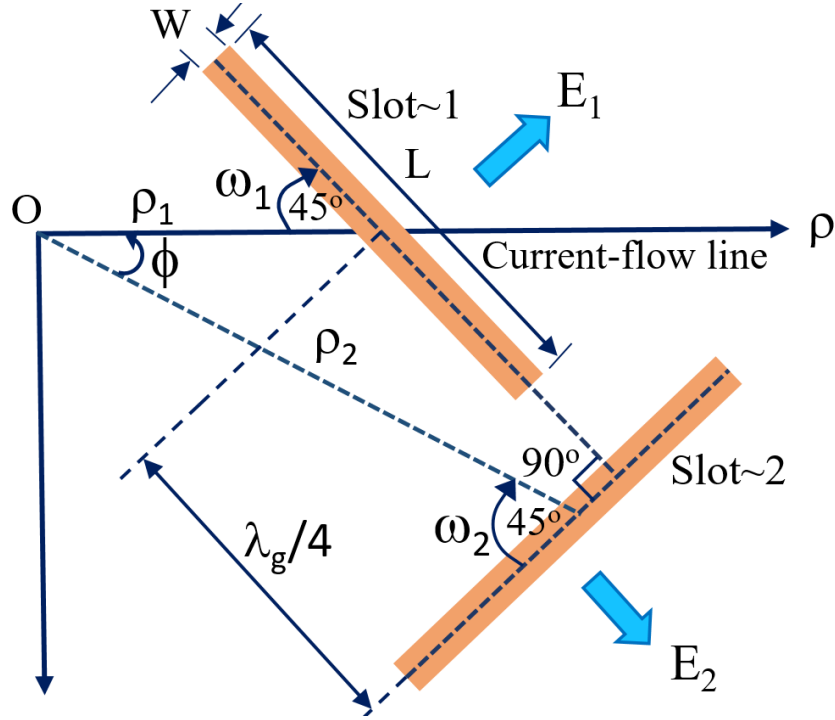
Figure 3.2: Two orthogonal slots configuration that acts as a unit radiator for CP-RLSA antenna.

ρ_2 : distance from the origin O to the centre of slot~2

ϕ : angle between slot~1 and slot~2

L : length of each slot

W : width of each slot

ω_1 : inclination angle of slot~1 with the current-flow line (a line drawn from the centre of the circular
     antenna towards the edge)

ω_2 : inclination angle of slot~2 with the current-flow line

In this unit radiator, the difference in the radial distance of the two slots from the origin gives the path
difference $(\rho_2 - \rho_1)$. This provides an excitation phase difference between the two slots, which can be
written as follows:

$$\text{Phase difference } (\triangle \phi) = (2\pi / \lambda_g) \times (\rho_2 - \rho_1) \tag{3.7}$$

where λ_g is the guided wavelength in the cavity of the antenna. To obtain circular polarisation, as
stated in equation 3.6, the phase difference must be equal to $\pi/2 + n\pi$ for CW rotation. This can be

simplified in the following way:

$$\pi/2 + n\pi = (2\pi/\lambda_g) \times (\rho_2 - \rho_1) \tag{3.8}$$

$$\therefore \rho_2 - \rho_1 = \lambda_g/4 \text{ [if n = 0]} \tag{3.9}$$

Equation 3.9 indicates that the difference in distances from one slot's centre to another slot's centre must be one-fourth of the guided wavelength. If the two slots are excited with equal amplitude and a relative phase shift of $\pi/2$, then they act as a right-hand circularly polarised unit radiator. The phase condition can be written as [5]:

$$arg(H_1^{(2)}(k\rho_2)) - arg(H_1^{(2)}(k\rho_1)) = \pi/2 \tag{3.10}$$

where arg(x) represents the phase of x, $H_1^{(2)}(k\rho)$ is the Hankel function of the second kind of order one, and $k = 2\pi/\lambda_g$ is the wave number in the radial waveguide. Furthermore, the requirement for circular polarisation leads both slots to be inclined at an equal angle to the current flow line. That is:

$$\omega_1 = \omega_2 = 45° \tag{3.11}$$

The spacing between two adjacent slot pairs in the radial direction (S_ρ) and in the azimuth direction (S_ϕ) should be smaller than the free space wavelength (λ_o) in order to avoid grating lobes from the slot array. In this design, the value of S_ρ is chosen around one guided wavelength and S_ϕ as half of the free-space wavelength in order to retain high aperture efficiency. All slot widths are the same over the aperture, while the length of each slot pair increases with the radial distance away from the centre. As the two slots in a pair are spaced $\lambda_g/4$ apart, the reflected waves from each slot are out of phase and cancel each other. In order to stabilise the travelling-wave mode, an area of radius P_{min} in the centre is left devoid of slots. The main parameters for designing the slot surface are given in Table 3.1. Using these design parameters the slot layout was created using Visual Basic (VBA) macros in CST Microwave Studio (documented in Appendix B). These macros automatically generate the slot layout on the top plate for a uniform aperture distribution.

Table 3.1: Parameters of the slot surface design configuration.

Free-space wavelength (λ_0) (mm)	15
Dielectric permittivity (ϵ_r)	1.41
Guided wavelength (λ_g) (mm)	12.6 ($\lambda_0/\sqrt{\epsilon_r}$)
Maximum aperture diameter (mm)	400 ($26.7 * \lambda_0$)
Slot length (L) (mm)	4.12 - 5.56
Slot width (W) (mm)	1 ($\lambda_0/15$)
Slot depth (mm)	0.035 ($0.002 * \lambda_0$)
Adjacent slot pairs spacing along ρ direction (S_ρ) (mm)	12 ($\lambda_0/1.25$)
Adjacent slot pairs spacing along ϕ direction (S_ϕ) (mm)	7.5 ($\lambda_0/2$)
Initial radius (ρ_{min}) (mm)	15 ($1 * \lambda_0$)
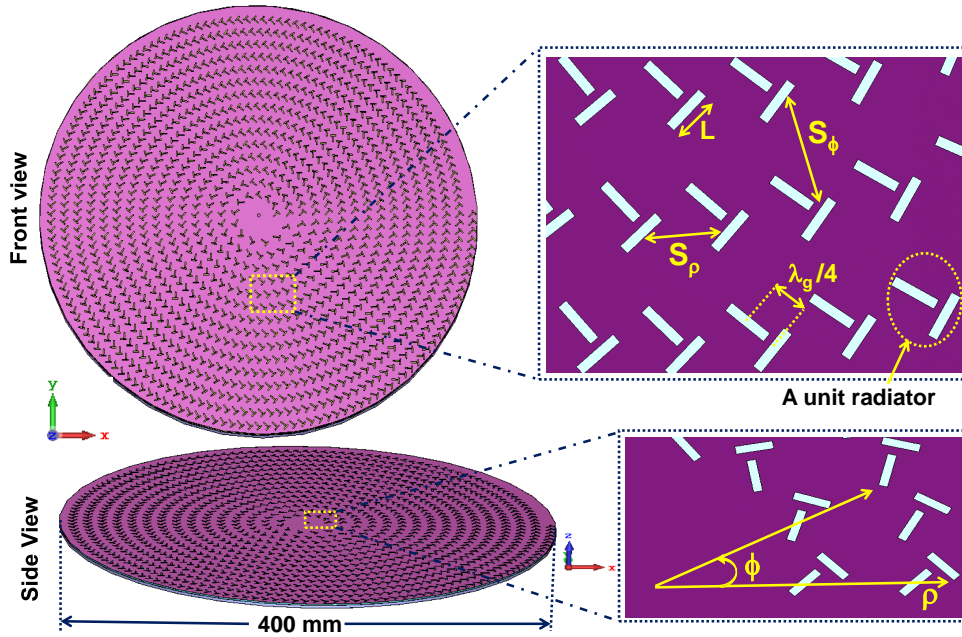
Figure 3.3: The final slot distribution of CP-RLSA antenna. The front and side view show the spirally arranged slot patterns, adjacent slot pairs spacing, and their orientations.

The final distribution of slots creates a spiral arrangement as shown in Figure 3.3. The direction of the spiral defines whether the field radiated is left-hand circularly polarised or right-hand circularly polarised.

3.3.2 Cavity Design

The second step in the CP-RLSA antenna design process is to model the waveguide cavity. To explain the mechanism of a radial waveguide, a single-layer cavity is shown in Figure 3.4. A coaxial cable is inserted as a transmission line from the bottom to feed the cavity. The cable has a disc head, which converts the power from the transverse electromagnetic (TEM) coaxial mode into the TEM cavity mode. The slots on the top plate couple the radial currents travelling outward within the cavity. The coupling of the slots is determined by the magnetic field within the waveguide. The energy not coupled by the slots escapes the cavity or can be absorbed by absorbing material placed at the edges. If the height of the waveguide (d) is less than one-half of the guided wavelength (d $< \lambda_g/2$), then the only possible symmetrical mode travelling within the cavity is the TEM mode whose magnetic field is given by [16]:

$$H_\phi(\rho) = H_1^{(2)}(k\rho) - \tau \frac{H_1^{(2)}(k\rho_{max})}{H_1^{(1)}(k\rho_{max})} H_1^{(1)}(k\rho) \tag{3.12}$$

where ρ = Radial position

$H_1^{(1)}(k\rho)$ = Hankel function of the first kind of order one

$H_1^{(2)}(k\rho)$ = Hankel function of the second kind of order one

τ = Reflection coefficient for the interface at the cavity edge of the antenna

In equation 3.12, the first term represents the outward travelling waves produced by the coaxial feed probe and the second term represents the inward travelling waves radiated from the reflections at the cavity boundary. For a large aperture size, the power remaining at the edge is considerably small, so the cavity edge can be left open. Also, the inward travelling waves (second term) only contribute to cross-polarisation pattern and have no impact on co-polar radiation. Therefore, the reflection
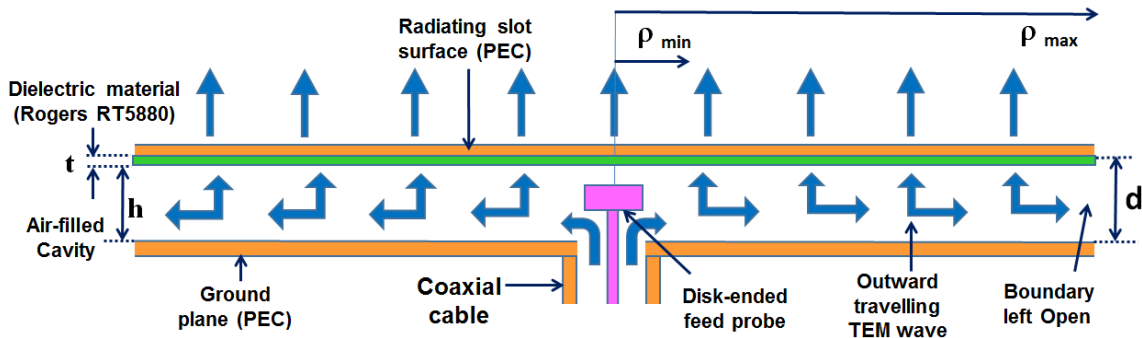
Figure 3.4: Pictorial representation of wave propagation inside the cavity and radiation from the surface of an RLSA antenna. The cavity is filled with a dielectric material and air.

coefficient is presumed to be negligible ($\tau \to 0$) and the second term in equation 3.12 is neglected to give:

$$H_\phi(\rho) \approx H_1^{(2)}(k\rho) \tag{3.13}$$

If $k\rho \gg 1$, we can simplify the equation as

$$H_\phi(\rho) \approx \sqrt{\frac{2}{\pi k P}} e^{-j(k\rho - 3\pi/4)} \tag{3.14}$$

Consequently, the slot excitation (equivalent magnetic current) is proportional to the inner field (F), whose variation within the radial distance can be approximated by [16]

$$F(\rho) \propto e^{-jk\rho} \tag{3.15}$$

Since the field has only a ϕ component, the only existing surface current is the radial current, proportional to H_ϕ.

In this design, the height (d) of the waveguide is optimised to 4.575 mm which is less than half of the guided wavelength ($\lambda_g/2 \approx 6.3$ mm). The choice of dielectric constant is a critical factor in designing the radial cavity. If the value of this dielectric constant is very small, grating lobes start appearing in the pattern. On the other hand, if the dielectric constant is too large, the antenna shows narrowband behaviour. Subsequently, the dielectric constant for designing the cavity is optimised to $\epsilon_r = 1.41$ in order to compromise between the requirements of bandwidth and efficiency. It is, however, difficult to obtain a commercially available dielectric material with the desired dielectric constant. For this reason, the cavity is designed with two layers of dielectrics. The upper layer is Rogers RT5880 with thickness t and the remainder of the waveguide is filled with air with height h, as shown in Figure 3.4. The equivalent dielectric constant ($\epsilon_r = 1.41$) is obtained by combining these two materials. Table 3.2 summarises the material properties.

Table 3.2: Cavity design parameters.

Specifications	Materials	Thickness	Permittivity
Upper layer	Rogers RT5880	1.575 mm	2.2 (ϵ_1)
Bottom layer	Air	3 mm	1 (ϵ_2)

3.3.3   Feed Structure Design

The feed transition is composed of a modified dielectric-coated 50 Ω coaxial connector which is etched from the centre of the ground plane to the cavity. The cable consists of a disk-ended feed probe which launches the outward travelling TEM wave in the radial waveguide. The head disk is made of copper and completely resides within the air gap. Figure 3.5 shows a perspective view of the feed structure. The main requirement of the feed design is to achieve reflection coefficient of -10 dB or less. To ensure optimal power transfer a feed structure was designed and all the design parameters were optimised using the parametric analysis in CST Microwave Studio. Table 3.3 summarises the feed structure design parameters. The coaxial post and the disk head are made of copper, and the coaxial shield is made of Teflon. The diameter (W_1) and height (H_1) of the head disk have been varied to get the optimum performance.
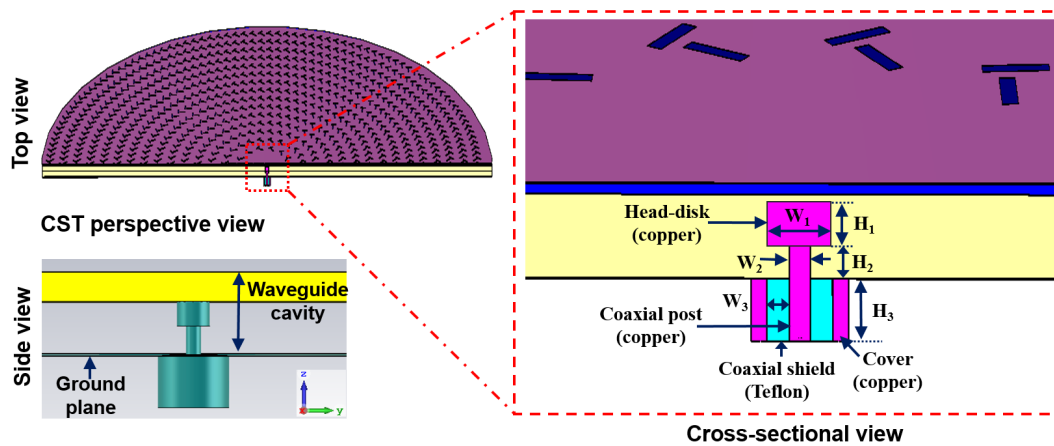
Figure 3.5: Feeding mechanism of a CP-RLSA antenna. The inset shows a cross-sectional view of a coaxial probe feeding.

Table 3.3: Feed structure design parameters.

Design parameters	Symbols	Values (mm)
Height of the disk head	H_1	2
Diameter of the disk head	W_1	3.6
Air gap below disk head	H_2	1.6
Diameter of the coaxial post	W_2	1.27
Width of the coaxial shield	W_3	2
Height of the coaxial shield	H_3	3

3.4   Numerical Results with Full-Wave Simulation

A design example of a CP-RLSA antenna, explained in the previous section, was simulated in CST Microwave Studio using the transient solver. Far-field results, as well as the matching of the antenna, were studied. Figure 3.6 shows the input reflection coefficient $|S_{11}|$ of the CP-RLSA antenna. It illustrates that the antenna is well matched within the operating band from 19 GHz to 24 GHz. As stated in Chapter 2, the CP-RLSA antenna has improved return loss characteristics, unlike an LP-RLSA antenna. This is because of the $\lambda_g/4$ inter-element spacing between two orthogonal slots in a unit radiator of the CP-RLSA antenna. The reflected waves from successive slots arriving back at the input port are out of phase and cancel each other. Since all the slot pairs are arranged spirally, the total sum of reflections is almost zero at the antenna feed point. Therefore, the antenna demonstrates excellent matching performance over the frequency band of interest. The 10-dB return loss bandwidth is 23.3%, which extends from 19 GHz to 24 GHz. The axial ratio in the broadside direction of the antenna is also shown in Figure 3.6. The axial ratio is lower than the 3-dB level over the operating frequency band, satisfying the standard CP condition.

Figure 3.7 shows the broadside directivity and gain of the antenna. The antenna has a peak directivity of 37.1 dBi with a peak gain of 36.9 dBi at 21.6 GHz. The gain variation is almost similar to that of the directivity over the entire operating frequency band. The total antenna efficiency is 95%, whereas the
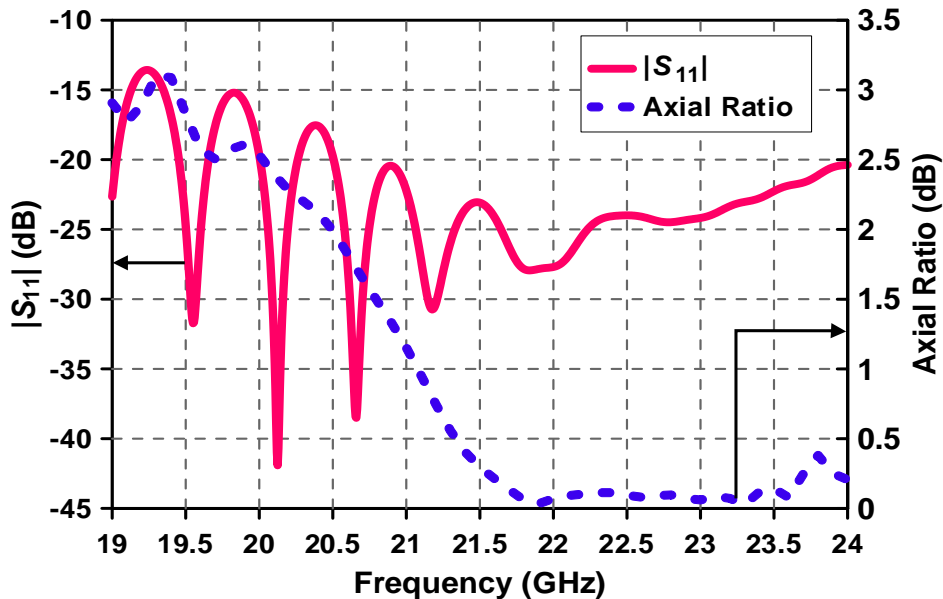
Figure 3.6: Input reflection coefficient and axial ratio in the broadside direction of CP-RLSA antenna.
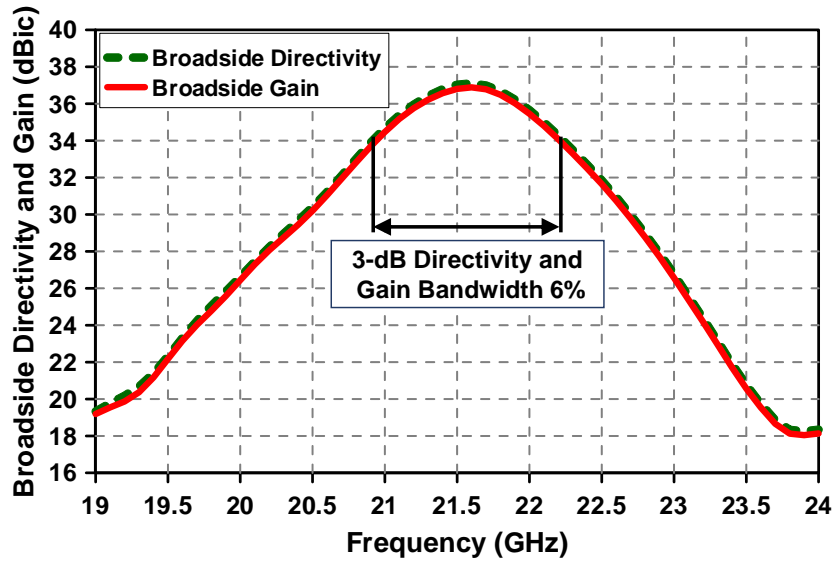
Figure 3.7: Broadside directivity and gain variation with frequency.

antenna has an aperture efficiency of 62.7%. This indicates that the antenna has achieved a satisfactory aperture illumination. The radiation efficiency of 95.4% was achieved at the frequency of peak gain. The antenna has demonstrated the 3-dB directivity bandwidth and 3-dB gain bandwidth of 6%, from 20.9 GHz to 22.2 GHz without any indicative difference between the directivity bandwidth and the gain bandwidth.

The radiation patterns at four different frequencies within the 3-dB gain bandwidth in the $\phi = 0°$ plane and $\phi = 90°$ plane are shown in Figure 3.8. All the radiation patterns show low sidelobe levels (SLLs) in both planes. The $\phi = 0°$ plane radiation pattern at the frequency of highest gain, i.e, at 21.6 GHz has SLL of -14.7 dB and the $\phi = 90°$ plane has an SLL of -12 dB. At frequencies of 20.9 GHz, 21.3 GHz, and 22.2 GHz, the $\phi = 0°$ plane has SLLs of -7 dB, -12.2 dB and -11.5 dB, respectively, whereas in the $\phi = 90°$ plane -8 dB, -8.4 dB and -15.5 dB, respectively.

Figure 3.9 compares the radiation patterns at frequency 21.6 GHz in both the $\phi = 0°$ plane and the $\phi = 90°$ plane along with the radiation pattern envelope (RPE)[1] for Class-2 and Class-3 antennas as specified by ETSI[2]. It is evident that the patterns in both planes have successfully met the requirements of the envelope trend.

---

[1]RPE plots the antenna's gain as a function of angle and provides a view of the antenna's directive properties. The corresponding RPEs as a function of (angle, gain (dBi)) for Class-2 antennas are (5, 20), (10, 12), (20, 10), (50, 2), (70, 0) and for Class-3 antennas are (5, 20), (10, 12), (20, 7), (40, 3), (50, 0). We have used these RPE values throughout the thesis for comparison.

[2]European Telecommunications Standards Institute, is the regulatory authority who sets strict requirements of the radiation patterns and gain for commercial compliant antennas.

(a)   (b)

(c)   (d)
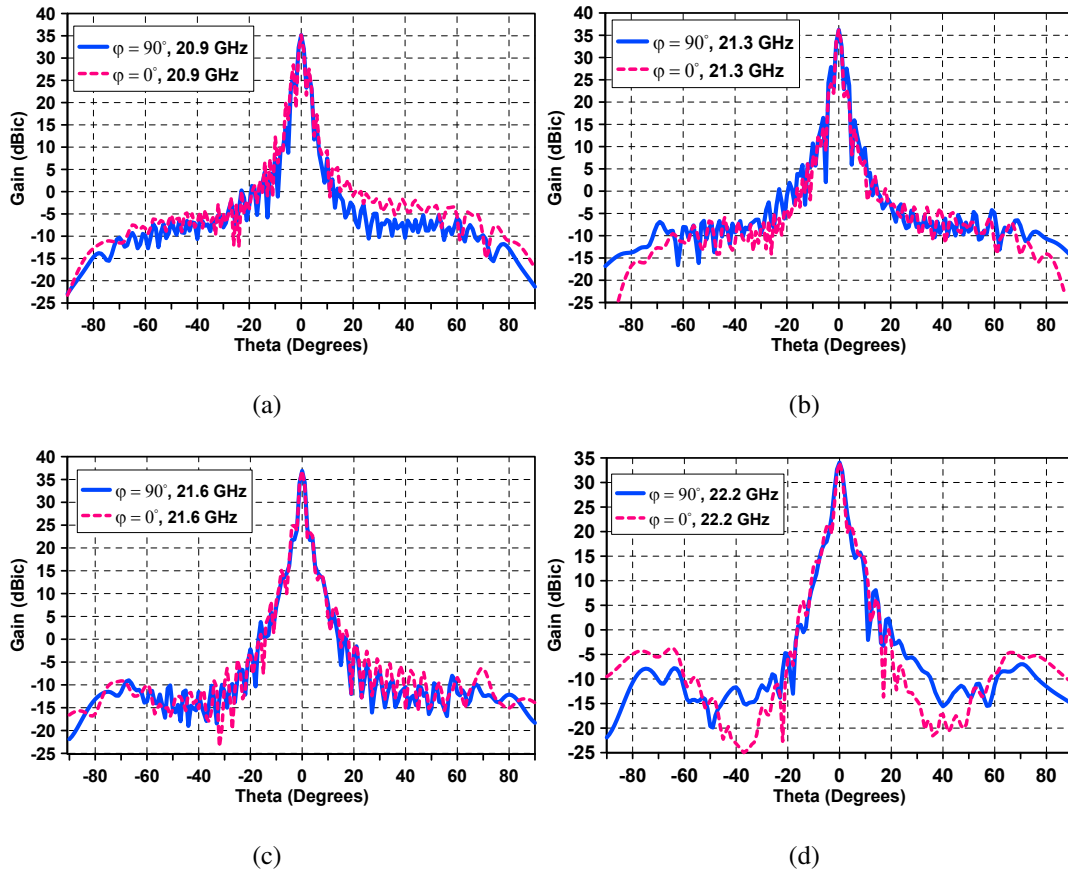
Figure 3.8: Radiation patterns of CP-RLSA antenna at (a) 20.9 GHz (b) 21.3 GHz (c) 21.6 GHz (d) 22.2 GHz.
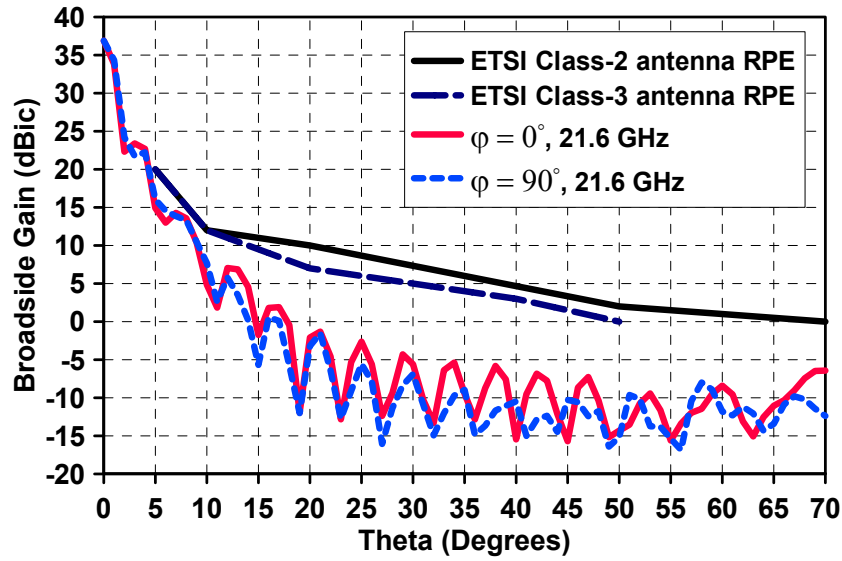
Figure 3.9: Comparison of radiation patterns of CP-RLSA antenna with ETSI-specified Class-2 and Class-3 RPEs at 21.6 GHz.

3.5   Summary

A detailed design methodology to model a CP-RLSA antenna has been discussed and is then used to design an optimised RLSA antenna. The antenna has demonstrated its potential to satisfy ETSI Class-2 and Class-3 antenna requirements with appropriate RPE values. A large return-loss bandwidth of 23.3% was achieved with the antenna. The antenna has demonstrated a peak directivity of 37.1 dBic and a peak gain of 36.9 dBic. The aperture and radiation efficiencies of this antenna are 62.7% and 95.4%, respectively. A significant improvement has been made in the sidelobe levels. The total thickness of the antenna is only $0.31\lambda_\circ$ (4.64 mm), which is smaller than for other planar high-gain antennas. The low profile and compact size of this antenna make it highly suitable for mobile satellite applications.

Chapter 4

RLSA Antennas with Uniform and Tapered Amplitude Distributions

4.1 Introduction

This chapter presents an investigation of CP-RLSA antennas with uniform and tapered amplitude distributions and evaluates the effects on pattern quality and radiation bandwidth. For this purpose, two CP-RLSA antennas are considered, each with different amplitude distributions but similar phase distributions. The distributions were obtained using slot coupling analysis on the aperture of RLSA antennas.

The strategy of controlling amplitude distribution through slot coupling is explained in Section 4.2. In order to demonstrate the working, two design examples are described in Section 4.3. Improvements in the antenna performance such as near-field phase uniformity, broadside directivity and gain, radiation patterns with controlled sidelobe levels are discussed in Section 4.4 to evaluate the performance of design examples.

4.2 Investigation of Electric Near-field Distribution

Slot coupling is the most important factor to control the aperture illumination in RLSA Antennas. The effect of slot coupling on the aperture illumination is explained in the following subsections.

4.2.1   Aperture Illumination

If slots are arranged on the aperture with equal length and width (uniform slots), then every slot will couple almost a constant factor proportion of the radial current. As the power is fed to the centre of the RLSA antenna, more power will radiate from around the centre and less power will radiate from the edges. Therefore, the power intensity of the outward travelling wave will be reduced by a factor of $1/\sqrt{\rho}$ through the radiative coupling of the slots, which is not favourable in terms of broadside gain. Therefore, a proper coupling control between the slots and the field is necessary to ensure that the illumination from the aperture is not steeply tapered. One possible method is to keep the slot surface density constant ($S_\rho \times S_\phi$ = constant) and control the power coupled by the slots from the inner cavity field to the radiating field. Strongly coupled slots can be placed on the outer part and weakly coupled slots in the inner part, to realise uniform illumination for efficiency improvement.

4.2.2   Synthesising Aperture Distributions

The excitation of the slots needs to be determined in order to have proper illumination from the aperture under the travelling-wave operation. The power coupling through the slots depends on two major design parameters: *i)* slot length (L), and *ii)* slot inclination angle (ω) with the current-flow line. For designing an RLSA antenna with circular polarisation, the slot inclination angles (ω_1, ω_2) are constant for all the slot pairs as given in equation 3.11. Therefore, the slot coupling is only controlled by manipulating the slot length over the aperture. The slot length can be varied along the radial distance to realise a uniform or non-uniform aperture illumination over the radiating surface. The slot length can be written as a function of radial distance [16] as

$$L_{slot} = \delta + (\rho \times \alpha) \tag{4.1}$$

where δ is a constant factor that depends on the operating frequency, ρ is the radial distance, and α is the coupling coefficient. δ needs to be optimised before creating the slot patterns. The term ($\rho \times \alpha$) acts as a coupling factor. For a particular design, the coupling coefficient α is optimised and then kept constant. As the radial distance increases, the coupling factor increases, that leads to increase the slot length. By controlling the coupling coefficient we can control the proportion of power coupled from the inner cavity field to the radiating field.

4.3   Design Examples

To investigate the influence of aperture illumination on the far-field performance, two circularly polarised RLSA (CP-RLSA) antennas were designed using: a) tapered amplitude distribution for lower sidelobe level and b) nearly uniform amplitude distribution for higher directivity and antenna efficiency. These two distributions were obtained by varying the slot length over the aperture and using the design procedure explained in Chapter 3. The two antennas were designed in the operating frequency ranges from 18 GHz to 22 GHz. The slot length design parameters of the two antennas are given in Table 4.1. In both antennas, the slot lengths are varied along the radial distance but at a different rate. The slot layouts were created using Visual Basic macros in CST Microwave Studio (documented in Appendix B) and shown in Figure 4.1. As can be seen from the figure, in the case of uniform amplitude distribution the slot lengths increase in the direction of ρ with an interval of

Table 4.1: Slot length design parameters.

Specifications	Constant factor (δ)	Radial distance (ρ)	Coupling coefficient (α)
Uniform amplitude	4	ρ	0.008
Tapered amplitude	4.8	ρ	0.004
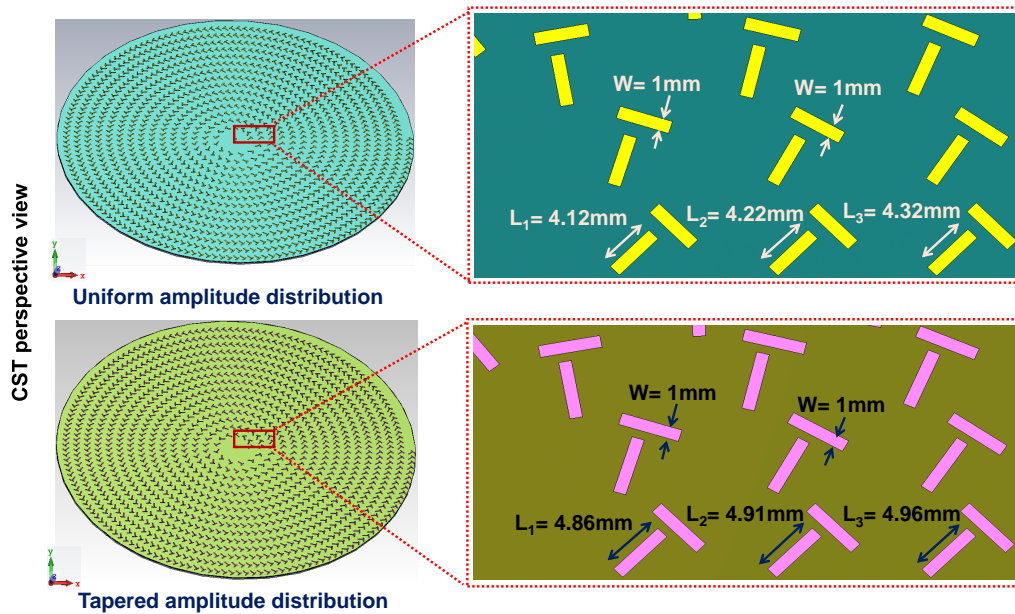
Figure 4.1: Final slot distributions on the surface of RLSA antennas for uniform and tapered illumination. L_n and W represent each slot length and width, respectively, where n = 1, 2, 3...

0.1 mm. However, in the case of tapered illumination the interval is 0.05 mm. The first slot has a length of 4.12 mm for the uniform and 4.86 mm for the tapered design. In both designs, all slots have a width (W) of 1 mm. The cavity and feed structure were designed as explained in Subsection 3.3.2 and Subsection 3.3.3 in Chapter 3. Numerical results are presented in the next section.

4.4   Numerical Results

The two designs were simulated using the transient solver of CST Microwave Studio. Both the near and the far-field results were analysed and are explained below.

4.4.1   Electric Near-Field Results

The electric near field was probed using post-processing templates in the full-wave solvers. For better understanding and analysis, amplitude as well as phase distributions were studied.

4.4.1.1   Amplitude Distribution

The amplitude distributions of the two designs at 20 GHz are shown in Figure 4.2. The patterns are taken in the XZ plane for the electric near field, extending from the top surface of the antenna to a distance of 8λ (120 mm above the top plate). The green line in Figure 4.2 (a) shows the tapered amplitude distribution with a peak at the antenna centre and gradually decreases towards the edges. On the other hand, the red line shows the uniform amplitude distribution, which is relatively uniform over
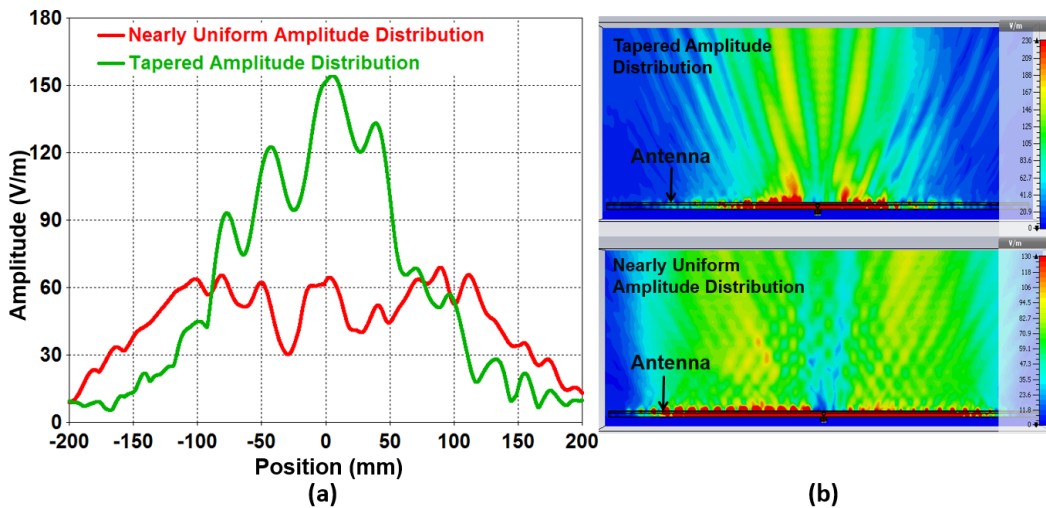
Figure 4.2: Amplitude distributions of the antennas for uniform and tapered illumination.

Phase of the antenna for uniform illumination

Phase of the antenna for tapered illumination
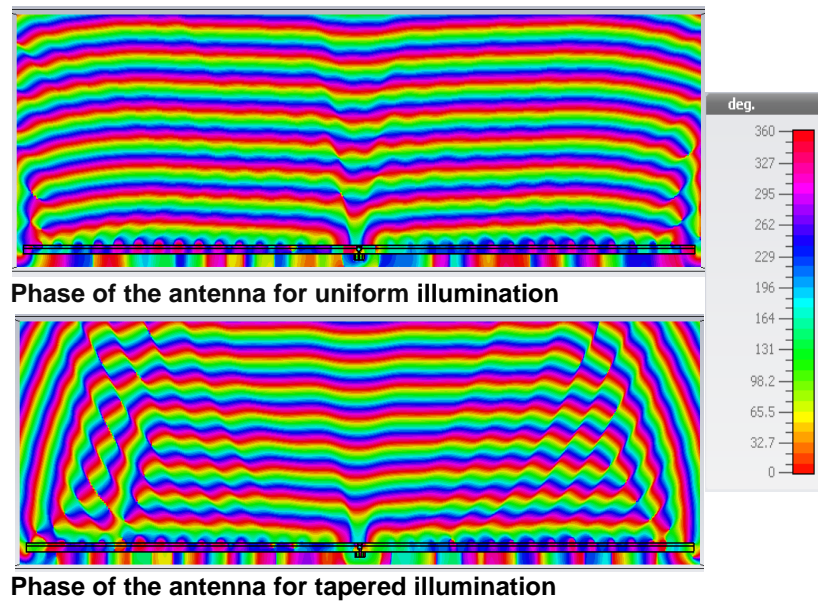
Figure 4.3: Phase distributions of the antennas for uniform illumination and tapered illumination.

the aperture. As can be seen from the electric near-field distribution in Figure 4.2 (b), with the tapered amplitude distribution more power is coupled to the slots near the centre, hence the illumination is stronger around the centre. With the uniform amplitude distribution, the illumination is nearly uniform throughout the aperture. This shows that the amplitude distribution can be tailored using the coupling coefficient.

4.4.1.2   Phase Distribution

The phase distributions of E_y, the electric field component in the H-plane, for the two designs are given in Figure 4.3. The figure illustrates a fairly uniform and symmetric phase distribution for the uniform illumination. On the other hand, the tapered illumination provides a nearly uniform phase with a slight deterioration around the antenna edges.

4.4.2   Far-field Results

The input reflection coefficients (S_{11}) for uniform and tapered illumination are shown in Figure 4.4. It can be seen that both designs have acceptable matching within the operating frequency band, with a predicted 10-dB return loss bandwidth of 20%, from 18 GHz to 22 GHz. The axial ratios for both distributions are also presented in Figure 4.4 as a function of frequency. Both designs demonstrate a
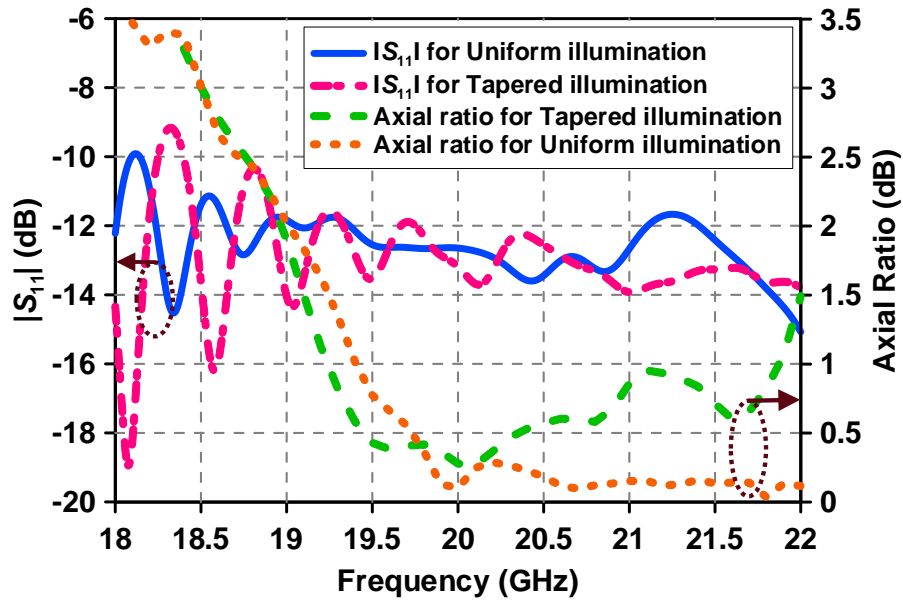
Figure 4.4: Input reflection coefficients (S_{11}) and axial ratios of uniform and tapered illumination.

very good axial ratio over the operating frequency band.

4.4.2.1 Aperture Distribution for Large Radiation Bandwidth

Figure 4.5 shows that with the uniform amplitude distribution, the directivity and 3-dB gain bandwidth have improved significantly as compared to the tapered distribution. The broadside directivity and gain at 20 GHz are 35 dBic and 34.5 dBic, respectively, with the uniform illumination. This corresponds to a total antenna efficiency of 90%. The antenna has demonstrated a relatively good 3-dB directivity
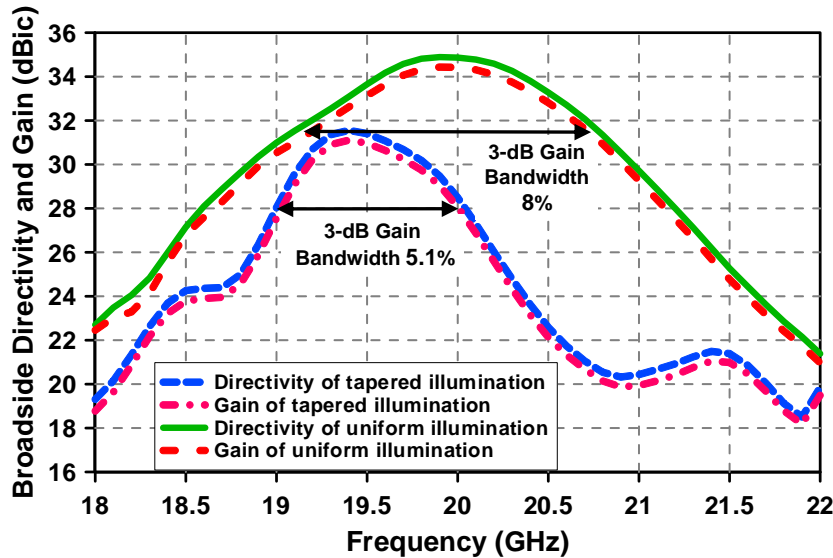
Figure 4.5: Measured broadside directivity and gain for uniform and tapered illumination.

bandwidth and 3-dB gain bandwidth of 8%, from 19.1 GHz to 20.7 GHz, which is very challenging to obtain in RLSA antennas with directivity >30 dBic. As shown in Figure 4.5, the tapered amplitude distribution gives a peak directivity of 31.6 dBic and a peak gain of 31.1 dBic at 19.4 GHz, along with a 3-dB directivity bandwidth and 3-dB gain bandwidth of 5.1%, from 19 GHz to 20 GHz. The total antenna efficiency, measured with tapered illumination, is 90%. The uniform amplitude distribution has achieved a 45% aperture efficiency, compared with 22% achieved using the tapered amplitude distribution. The radiation efficiencies are almost identical for the two designs ($\approx$95%).

4.4.2.2   Aperture Distribution for Lower SLLs

Although the tapered aperture distribution presents a reduced 3-dB gain bandwidth and a lower peak gain, but the sidelobe levels (SLLs) has improved significantly as compared to the uniform distribution as shown in Figure 4.6. The sidelobe levels are plotted along $\phi = 0°$ plane. It can be seen that the lowest SLL at the frequency with peak gain, achieved with uniform illumination, is -10.3 dB at 20.0 GHz. On the other hand, with tapered illumination, the lowest SLL is -26.1 dB at 19.4 GHz. Figure 4.7 shows the far-field radiation patterns in the $\phi = 0°$ plane and $\phi = 90°$ plane for tapered and uniform aperture distributions, to compare with ETSI Class-2 and Class-3 antennas' RPEs. The SLLs, with uniform illumination, are predicted to be -10.3 dB and -13 dB in the $\phi = 0°$ plane and $\phi = 90°$ plane, respectively, at 20 GHz. With the tapered illumination, the SLL has significantly reduced to -26.1 dB in the $\phi = 0°$ plane and -23 dB in the $\phi = 90°$ plane at 19.4 GHz. Both antennas have effectively met the requirements of ETSI Class-2 and Class-3 antennas with the appropriate radiation pattern envelope (RPE) values as illustrated in Figure 4.7.
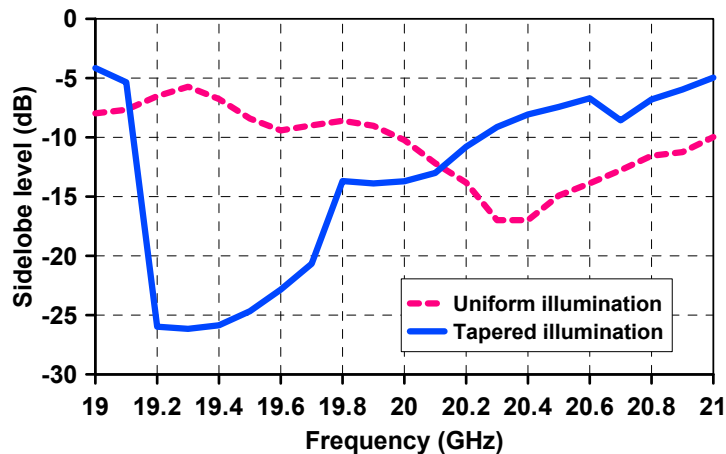
Figure 4.6: Sidelobe levels for tapered and uniform aperture distributions.
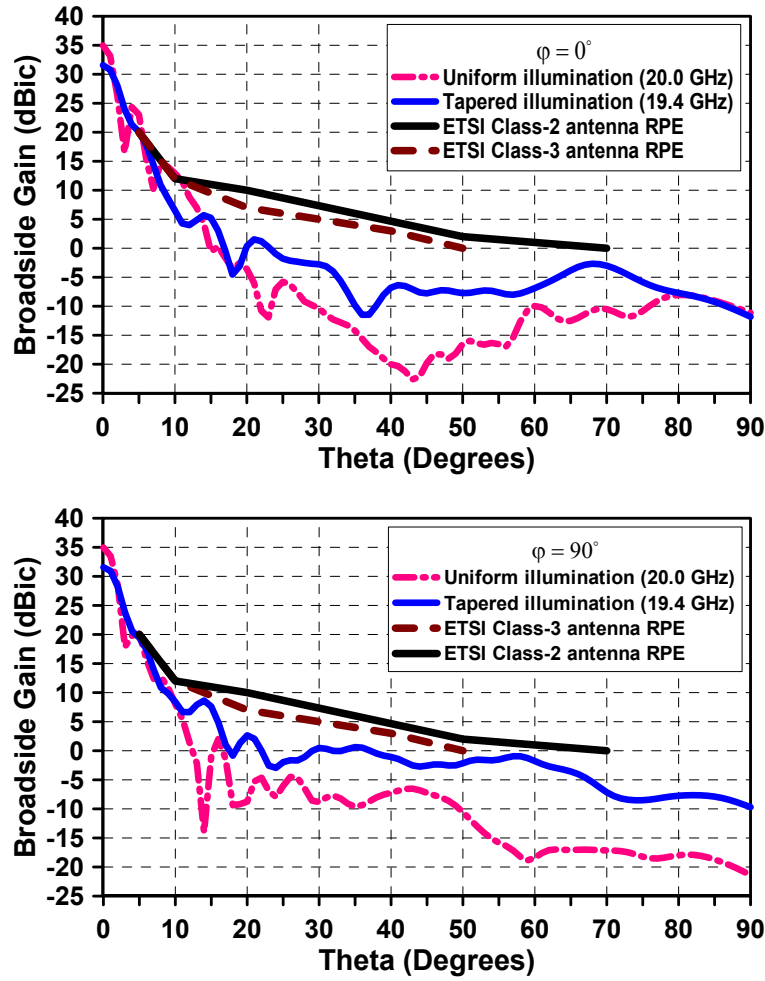
Figure 4.7: Far-field radiation patterns for the tapered and uniform aperture distributions, comparing with ETSI Class-2 and Class-3 antennas' RPE values in the $\phi = 0°$ plane and $\phi = 90°$ plane.

4.5   Summary

In this chapter, we have investigated two field distributions (uniform and tapered) of single layer CP-RLSA antennas. The distributions were obtained by controlling the slot coupling as a function of radial distance. This method relies on the fact that the power coupled by the radiating slots is a function of the slot's length and, by changing the length of the slots over the radiating surface, uniform and tapered field distributions can be achieved. The numerical results demonstrated that the uniform amplitude distribution provides a peak broadside directivity of 35 dBic with a 3-dB gain bandwidth of 8%. The tapered amplitude distribution provides a lower gain (3.4 dB less) and smaller 3-dB gain bandwidth (2.9% less) but with better sidelobe levels (SLLs), as low as -26.1 dB. Both antennas have met the requirements for ETSI Class-2 and Class-3 antennas' RPEs.

Chapter 5

Radiation Bandwidth Improvement of RLSA Antennas

5.1   Introduction

The CP-RLSA antennas presented in the previous two chapters demonstrate highly directive radiation beams and high radiation efficiencies with low sidelobe levels. However, one of the main limitations of RLSA antennas is their narrow radiation bandwidth[1]. There are several applications requiring a wide radiation bandwidth with high gain. In this chapter, a new design configuration of the RLSA antenna cavity is proposed to increase the radiation bandwidth.

The permittivity of the dielectric material which partially fills the cavity is changed as a function of radial distance from the centre to the edge. This variation is achieved by replacing the uniform dielectric layer (as described in Chapter 3) with rings of various dielectric materials. The rest of the RLSA configuration remains the same, as discussed in previous chapters. This new cavity configuration, with reference to classical cavities, is explained in Section 5.2. An RLSA antenna design using the proposed configuration is described in Section 5.3. Full-wave simulation results are given in Section 5.4 to validate the concept.

5.2   Proposed Cavity Design to Achieve Wideband

Since the RLSA is a travelling wave antenna, the radiation bandwidth is limited by the waveguide length, especially for large antennas. Resonance of the slots also limits the bandwidth of RLSA

---

[1]Radiation bandwidth is the bandwidth in which the gain remains within 3-dB of the peak value.

antennas. The relative permittivity (ϵ_r) of the dielectric material has a massive effect on the radiation bandwidth of RLSA antennas. Let us investigate the effect of having non-uniform relative permittivity of the dielectric materials filling the cavity. This variation of the relative permittivity results in changing the wave propagation inside the cavity, which effects the effective electrical length of the waveguide. The new cavity configuration with permittivity variation is explained in the following subsection.

5.2.1 Cavity Configuration

The configuration of the proposed RLSA antenna cavity is shown in Figure 5.1. The cavity is made of substrates with transverse permittivity gradients (STPG). Previously, STPGs have been used to design wideband resonant cavity antennas [39]. The rest of the waveguide is filled with air as described in previous chapters. The STPG with circular aperture has a thickness (t) and is spaced a height (h) above the ground plane. The total radius R is equal to the radius of the top plate. The continuous gradient disc is divided into a number of segments as shown in Figure 5.1. The STPG includes one small circle in the centre of the structure (width W_1), filled with air ($\epsilon_1 = 1$), and surrounded by annular rings one after another. Each ring has a width of W_r (where r = 2, 3,......N) and a relative permittivity, ϵ_i (where
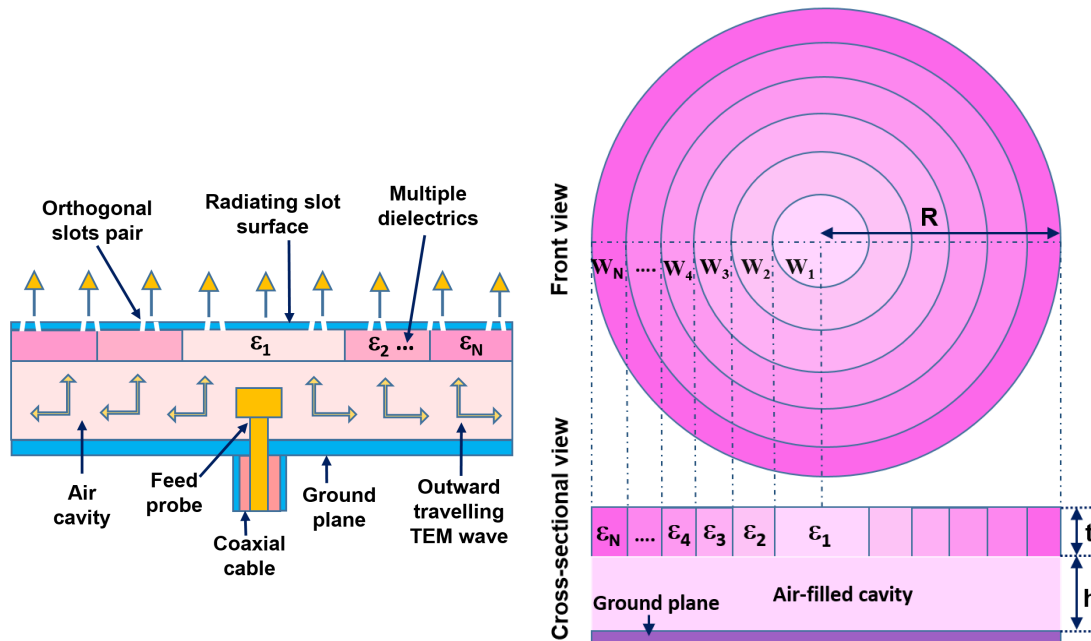
Figure 5.1: Example configuration of an RLSA antenna cavity using permittivity variation of the dielectric materials in the transverse direction: (Left) Cross-sectional view of the proposed RLSA antenna with STPG-loaded cavity; (Right) Front and side views of the STPG configuration.

i = 2, 3,......N). N defines the total number of quantised segments. In the centre of the antenna, the value of ϵ_i is the lowest and it gradually increases towards the edges, so that ϵ_N is the highest value. The width (W_r) of the segments may or may not be equal.

5.2.2 Comparison of the STPG-loaded Cavity with Conventional Cavity

In this work, the STPG has ten permittivity values and they are arranged in ascending order ($\epsilon_1 = 1, \epsilon_2 = 2, \epsilon_3 = 3, ...\epsilon_{10} = 10$) from the centre towards the edges. The thickness (t) of the STPG is a critical factor to optimise the total height of the waveguide. As discussed in Section 3.3.2 in Chapter 3, the total height of the cavity should be less than one-half of the guided wavelength ($\lambda_g/2$) to ensure the propagation of the TEM wave. In this design, the thickness (t) of the STPG is optimised to 0.5 mm. The air-gap height (h) is set to 5 mm. Therefore, the total waveguide height is 5.5 mm (0.5+5), which is less than half of the guided wavelength ($\lambda_g/2 = 12.6/2 = 6.3$ mm). All segment widths were kept equal ($W_1 = W_2 = W_3 = ...W_N$). The radius of the antenna is 200 mm. Therefore, each segment width is 20 mm.

The slotted surface was designed with uniform amplitude distribution as explained in Chapter 4. The thickness of the top PEC plate is 1 mm and the feed transition consists of a coaxial probe terminated in a disk-shaped stub, as described in Chapter 3. Figure 5.2 shows the broadside directivity of the CP-RLSA antenna with the STPG-loaded cavity compared with the directivity obtained from classical cavities having uniform dielectric materials. The relative permittivity (ϵ_r) of the uniform dielectric
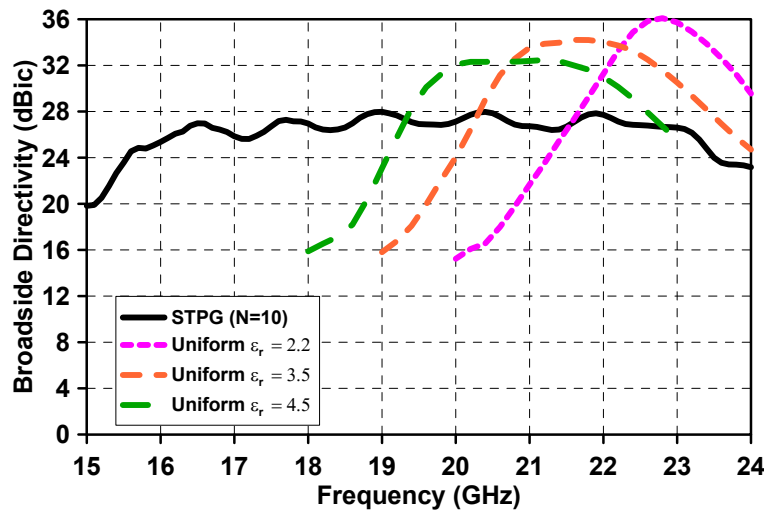
Figure 5.2: Comparison of the 3-dB directivity bandwidth between STPG-loaded (N=10) cavity and uniform substrates with different permittivity values.

materials are 2.2, 3.5, and 4.5, which are commercially available. All the design parameters such as total radius (R), the substrate thickness (t), air cavity height (h) are kept constant for all designs. It can be seen from Figure 5.2 that with the STPG-loaded (N=10) cavity, the bandwidth has increased notably over the uniform ones. The 3-dB directivity bandwidth of the antenna loaded with STPG cavity is from 15.8 GHz to 23.4 GHz. It was found that, with the increase in relative permittivity for each uniform substrate, the peak directivity decreases, whereas the directivity bandwidth increases. The effect of the quantisation level is further studied and explained in the following subsection.

5.2.3 Effect of Quantisation Level

Extensive simulations were carried out to investigate the effects of the quantisation level (N) on antenna performance. Specifically, the 3-dB directivity bandwidth and peak directivity within the operating frequency band were evaluated. Table 5.1 summarises the antenna's performance. It can be seen that, for N = 10, the 3-dB directivity bandwidth is 38.8% with a peak directivity of 28 dBic. As the value of N decreases, the bandwidth gradually decreases but the directivity increases. To study the effect of the permittivity values for a fixed quantisation level we have designed two CP-RLSA antennas with the same quantisation level: N = 5. The results are summarised in Table 5.1. The lower-permittivity material set (1, 2, 3, 4, 5) provides better antenna performance than the higher-permittivity material set (1, 3, 5, 7, 9) in terms of directivity and bandwidth. For this reason, the lower permittivity materials are used when designing the STPG configuration and lower N for ease of manufacturing.

With N = 4, the 3-dB directivity bandwidth reaches 19.4% with a reasonable directivity of 32.5 dBic.

Table 5.1: Antenna performance for different numbers of quantisation levels.

Quantisation level (N)	Relative permittivity $\{\epsilon_1, \epsilon_2, ...\epsilon_N\}$	3-dB directivity bandwidth (%)	Peak directivity (dBic)
10	1, 2, 3, 4,.....8, 9, 10	38.8	28
5	1, 3, 5, 7, 9	24	29.8
5	1, 2, 3, 4, 5	20	32.2
4	**1, 1, 3, 4.5**	**19.4**	**32.5**
1	4.5	12	32.4
1	3.5	10	34.1
1	2.2	6	36

In addition to the proposed cavity configuration, the table also exhibits the 3-dB directivity bandwidth and peak directivity of conventional RLSA antennas having cavities with uniform substrates. It can be seen that, as the value of the relative permittivity of the uniform substrate decreases, the peak directivity increases, with a reduction in the bandwidth. Compared with the uniform substrates and larger N, the STPG with quantised level N = 4 provides a good compromise between the directivity and the enhanced 3-dB directivity bandwidth.

5.3   Design Example

Based on the results obtained from Table 5.1, we have designed a CP-RLSA antenna with the new STPG cavity for quantisation level N = 4. The antenna was designed for an operating frequency of 20 GHz (λ_o = 15 mm). The top plate has the slot pattern and the bottom plate is the ground plane made of copper. The radius of the cavity, slot plate and ground plane are the same, i.e. R = 200 mm ($\approx 13.3\lambda_o$). The cavity with the STPG structure is divided into four segments, where each segment has the following width: $W_1 = W_2 = W_3 = W_4 = 50$ mm. The first two segments near the centre
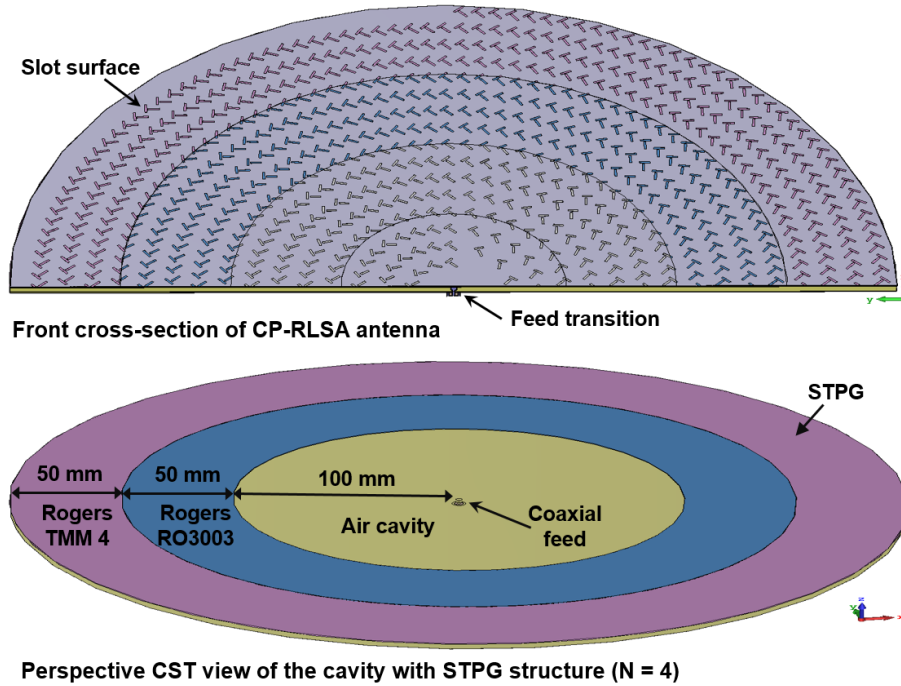
Figure 5.3: CP-RLSA antenna with STPG-loaded (N = 4) cavity. The cavity is divided into four segments with equal width, where the first two segments are filled with air and the last two segments are made of dielectric materials.

are filled with air ($\epsilon_1 = \epsilon_2 = 1$). The next two segments are composed of commercially available dielectric materials of Rogers RO3003 and Rogers TMM 4 with relative permittivities of $\epsilon_3 = 3$ and $\epsilon_4 = 4.5$, respectively. The loss tangents of these two materials are 0.001 and 0.002, respectively. The thickness of the slot surface and ground plane is 1 mm. The air-filled cavity height (h) is set to 4 mm. The thickness (t) of every segment of the STPG is optimised to 0.5 mm. The waveguide with STPG and air cavity gives an equivalent dielectric constant of $\epsilon_{equ} = 1.1549$. The guided wavelength (λ_g) is 13.95 ($\lambda_o/\sqrt{\epsilon_{equ}}$). Therefore, the total waveguide height 4.5 mm (0.5+4), is less than half of the guided wavelength 6.97 mm ($\lambda_g/2$), which ensures that only the TEM wave propagates inside the waveguide cavity. The slot configuration on the top plate is laid out to achieve uniform illumination as described in Chapter 4. The feed-structure design parameters are the same as in Table 3.3 in Chapter 3. Figure 5.3 shows the final configuration of the CP-RLSA antenna with STPG-loaded cavity.

5.4 Full-Wave Simulation Results

The antenna was simulated with the time-domain solver in CST Microwave Studio for frequencies from 19 GHz to 25 GHz to verify the design. Figure 5.4 shows the return loss performance of the antenna. It can be observed that the antenna is well matched over the entire frequency band. The antenna has demonstrated a 10-dB return loss bandwidth of 27.3%, extending from 19 GHz to 25 GHz. The axial ratio of the antenna in the broadside direction is also presented in Figure 5.4. The axial ratio
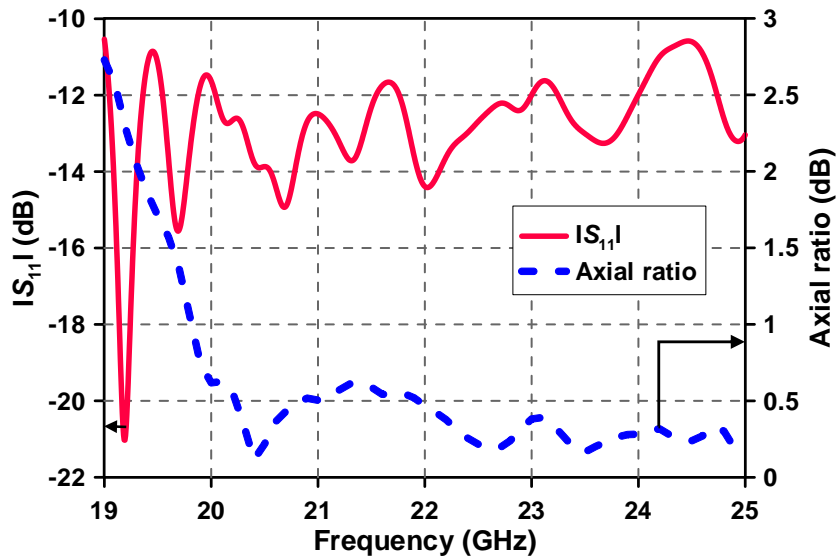
Figure 5.4: Reflection coefficient and axial ratio of the CP-RLSA antenna with the STPG-loaded cavity.

is below the 3-dB level over the entire frequency band. This shows that the proposed antenna exhibits circular polarisation of good quality.

Figure 5.5 shows the broadside directivity and gain of the CP-RLSA antenna. The antenna has a
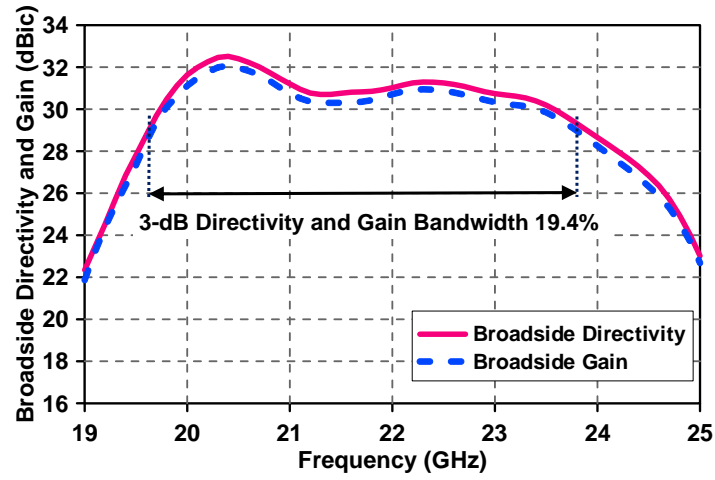
Figure 5.5: Broadside directivity and gain of the antenna with the STPG-loaded cavity.
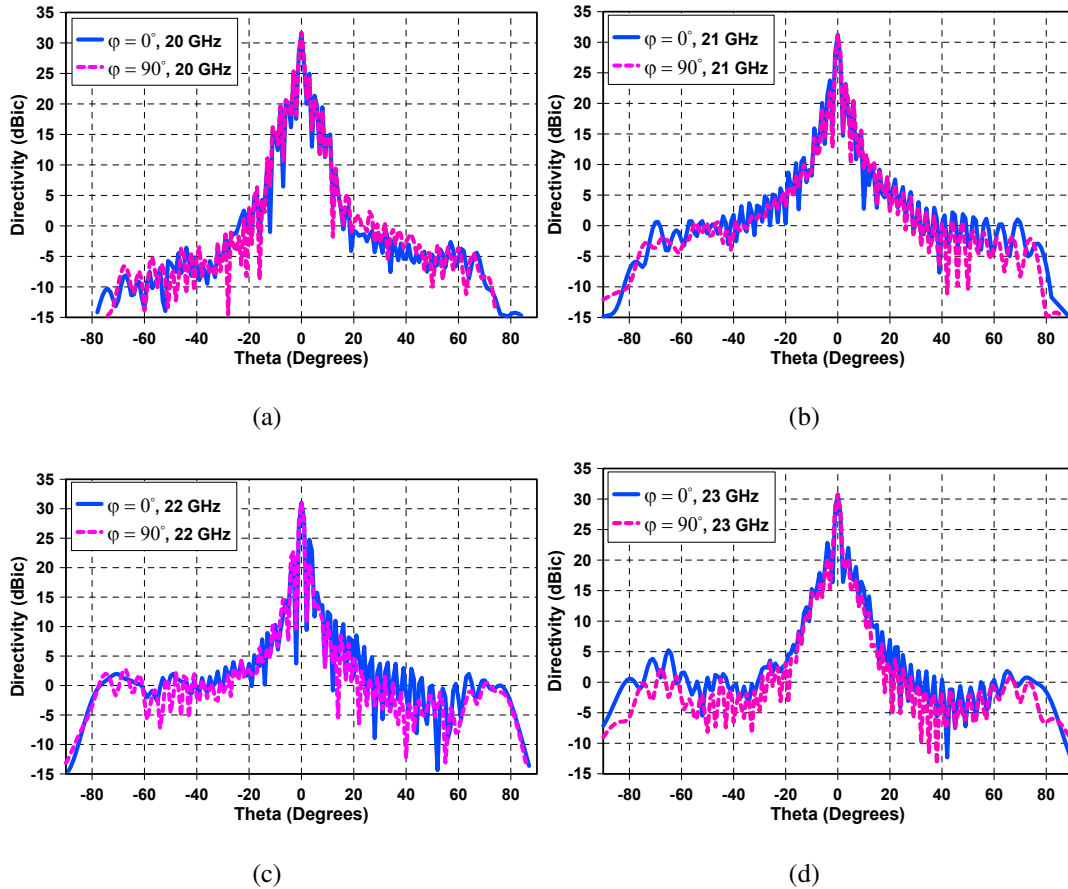
Figure 5.6: Radiation patterns of the antenna at (a) 20 GHz (b) 21 GHz (c) 22 GHz (d) 23 GHz.

peak directivity of 32.5 dBic and a peak gain of 32 dBic at 20.4 GHz. An excellent improvement can be observed in the half-power gain bandwidth of the antenna with only four-segmented STPG (N = 4) cavity. The 3-dB directivity bandwidth and 3-dB gain bandwidth measured 19.4% extending from 19.6 GHz to 23.8 GHz. The directivity bandwidth complements the gain bandwidth without any significant difference. The total antenna efficiency obtained was 90%, whereas the radiation efficiency reached 94% at 20.4 GHz. Since no absorber is placed at the edges, the antenna efficiency is higher than conventional RLSA antennas.

The radiation patterns of the antenna in the broadside direction at four different frequencies are shown in Figure 5.6 within the 3-dB directivity bandwidth. It can be observed that the $\phi = 0°$ plane and $\phi = 90°$ plane exhibit nearly similar radiation patterns at all four frequencies. The radiation
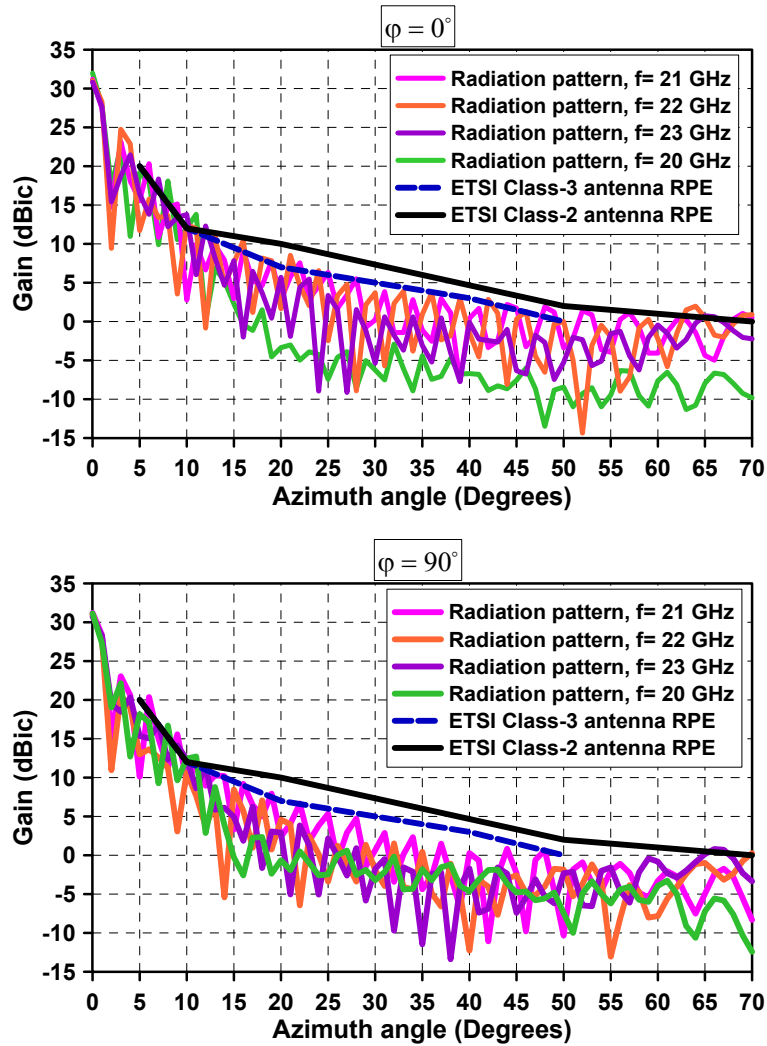
Figure 5.7: Comparison of the far-field radiation patterns of the antenna at four different frequencies with ETSI Class-2 and Class-3 antennas' RPE values in the $\phi = 0°$ plane and $\phi = 90°$ plane.

patterns at these frequencies are compared with the RPE values of ETSI Class-2 and Class-3 antennas in Figure 5.7. Generally, both the $\phi = 0°$ plane and $\phi = 90°$ plane patterns followed the envelope except around the angles 5° and 10°, where the $\phi = 0°$ plane pattern exceeded the RPE to a maximum of 3 dB and the $\phi = 90°$ plane pattern exceeded the RPE to a maximum of 1.9 dB.

5.5   Discussion

The STPG cavity is a convenient approach to increases the 3-dB directivity and gain bandwidth of the RLSA antenna. As discussed in previous sections, the bandwidth enhancement is often accompanied by a decrease in the peak gain. Some more configurations to obtain high gain with wide directivity bandwidth is shown in Table 5.2. Each of these configurations consists of an equal number of STPG segments, N = 4 (200 mm radius) but with different permittivity values. The segments are composed of commercially available dielectric materials including foam ($\epsilon = 1.12$). As can be seen from the table, with the variation of permittivity values the peak directivity and the 3-dB directivity bandwidth can be controlled to obtain the desired directivity or bandwidth values. The 3-dB directivity bandwidth has increased more than 6% in each of the design with the STPG-loaded cavity as compared to conventional uniform substrates [13, 14, 16, 22].

Table 5.2: Antenna performance with equal segmentation of STPG cavity.

Segment number (N)	Relative permittivity $\{\epsilon_1, \epsilon_2, \epsilon_3, \epsilon_4\}$	Peak directivity (dBic)	3-dB directivity bandwidth (%)
4	1.12, 1.96, 2.2, 2.33	35	11.4
4	1, 1, 1.12, 1.96	34.6	13.8
4	1, 1.12, 1.96, 2.2	34	15.8

5.6   Summary

In this chapter, we presented a new cavity design methodology to increase the radiation bandwidth of RLSA antennas. We analysed the antenna cavity operation with an STPG structure using full-wave simulation. Numerical results predict an increase in the 3-dB directivity bandwidth and 3-dB

gain bandwidth of 19.4% with a peak directivity of 32.5 dBi. This figure represents a tremendous improvement in the directivity and gain bandwidth of RLSA antennas. The arrangement of the STPG in the waveguide cavity minimises the effect of reflections from the adjacent slots on the radiating surface. This assists the antenna to achieve a very good return loss bandwidth of 27.3%. The total thickness of this new proposed antenna is only $0.43\lambda_\circ$ (6.5 mm) which is very small compared with other planar antennas, helping it to fit easily everywhere.

Chapter 6

Beam Steering of RLSA Antenna using Metasurface

6.1 Introduction

In the previous chapters, our main focus was to enhance the radiation bandwidth and improve the radiation patterns of CP-RLSA antennas. In terms of the direction of radiation, all of those RLSA antennas have a radiation beam fixed in the broadside direction. To accommodate applications such as communication-on-the-move (COTM) and satellite reception, requiring high-gain antennas with beam-steering features. The RLSA antenna is a suitable option for such applications because of its high gain and planar profile, but they lack the beam-steering technique. In this chapter, we present a beam-steering RLSA antenna design. The design is accomplished by placing metasurfaces in the near field region of the RLSA antennas.

The detailed mechanism of the steering technique is explained in Section 6.2. The design procedure of the metasurface is described in Section 6.3 and the numerical results, obtained with the metasurface and RLSA antenna, are discussed in Section 6.4.

6.2 Beam Steering using Near-field Phase Transformation

Recently a method, based on the near-field phase transformation, has been used to design a planar beam-steering antenna system [40, 41]. This method was used to demonstrate a medium-gain resonant cavity antenna (RCA). However, in contrast to the previous work, we have used this method for a high-gain CP-RLSA antenna with a large aperture. The method requires a pair of phase-transforming

metasurfaces (each referred to as beam steering metasurface (BSM)). Each metasurface is placed in the near-field region of the RLSA antenna aperture. The metasurfaces transform the nearly uniform phase distribution of the RLSA antenna to a linearly progressive phase, thus changing the beam direction from broadside to an offset angle of γ as shown in Figure 6.1.

When one BSM rotates (orientation angle (β)) about its axis, the beam moves along the surface of a
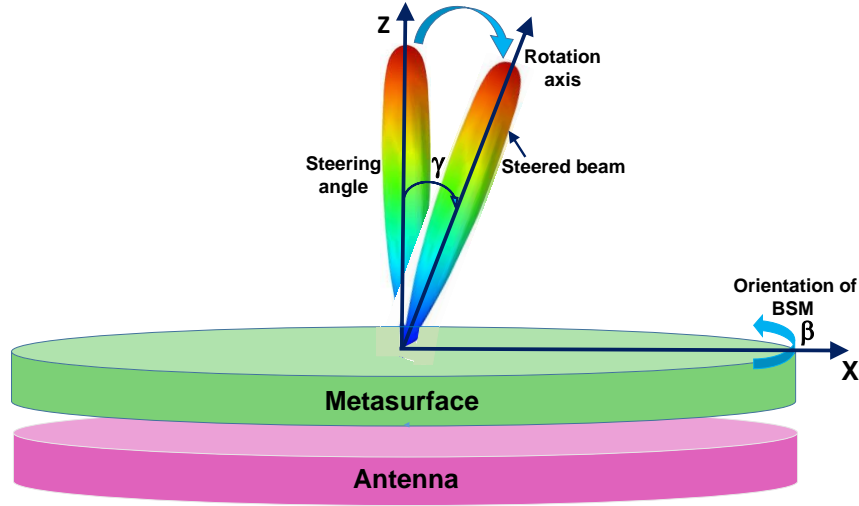
Figure 6.1: Beam-steering technique with near-field phase transformation. The main beam can be steered with a steering angle of γ using phase-shifting mechanism.

cone having a vertex angle of 2γ. The turning of a single BSM moves the beam in the azimuth plane for a fixed elevation angle. For complete 2D beam steering, two such BSMs are required and this is explained in the next section. Two identical BSMs are capable of steering the antenna beam in any direction within a conical region having a vertex angle of 4γ.

6.2.1   Beam Scanning using a Pair of BSMs

The working principle has been explained in details in [40, 41] and is briefly summarised below. We consider two beam steering metasurfaces (BSM_1 and BSM_2) placed on the top of an RLSA antenna as shown in Figure 6.2. BSM_1 and BSM_2 have fixed beam-tilt angles (γ_1, γ_2) and can have variable orientation angles (β_1, β_2), respectively. The resultant beam location is represented by elevation angle θ and azimuth angle ϕ. The beam position is controlled by the rotation of the two BSMs, i.e. by changing β_1 and β_2. The elevation angle (θ) is calculated directly using [41]:

$$\therefore \theta = \sqrt{\gamma_u^2 + \gamma_v^2} = \sqrt{\gamma_1^2 + \gamma_2^2 + 2\gamma_1\gamma_2 \cos(\beta_1 - \beta_2)} \tag{6.1}$$
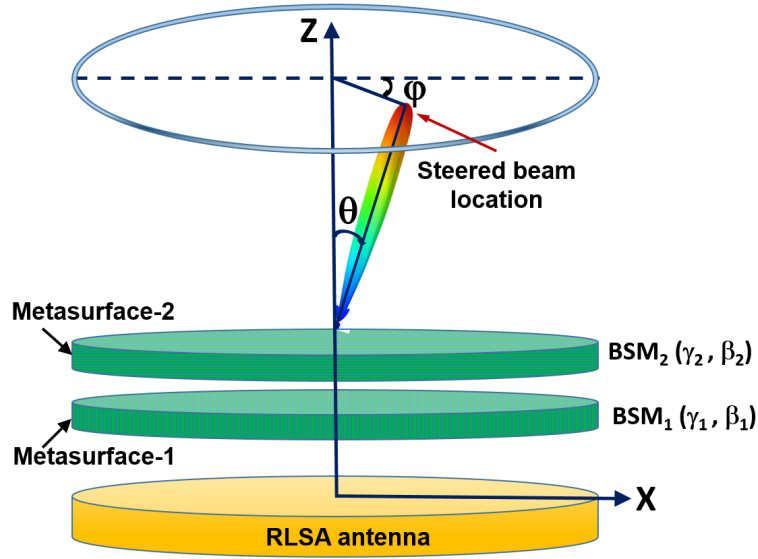
Figure 6.2: A pictorial view of a CP-RLSA antenna with two beam-steering metasurfaces. With co-rotation of the two BSMs, the beam can be steered. (θ, ϕ) represent the resultant beam position.

where, $\gamma_u = \gamma_1 \cos \beta_1 + \gamma_2 \cos \beta_2$

$\gamma_v = \gamma_1 \sin \beta_1 + \gamma_2 \sin \beta_2$

The azimuth angle (ϕ) is calculated using an intermediate value ϕ' as follows:

$$\phi' = \tan^{-1} \frac{\gamma_v}{\gamma_u} = \tan^{-1} \frac{\gamma_1 \sin \beta_1 + \gamma_2 \sin \beta_2}{\gamma_1 \cos \beta_1 + \gamma_2 \cos \beta_2} \qquad (6.2)$$

$$\phi = \begin{cases} \phi' & \gamma_u \geq 0, \gamma_v \geq 0 \\ 180^0 + \phi' & \gamma_u < 0 \\ 360^0 + \phi' & \gamma_u \geq 0, \gamma_v < 0 \end{cases} \qquad (6.3)$$

6.3   Beam-Steering Metasurface Design

The design of each BSM is based on antenna array theory. The total aperture, which is equal to the physical aperture of the RLSA antenna, is divided into a grid of square cells as shown in Figure 6.3. Each cell is treated as an antenna within a 2D array. The cell size used here is $\lambda_0/2 \times \lambda_0/2$ (7.5×7.5 mm). These cells of the BSM are assigned a phase shift so that the BSM can tilt the beam in the desired direction. In general, the beam is tilted along one of the linear axis (X-axis here). Therefore, the phase progressively increases along the X-axis and remains constant along the Y-axis. The phase-shift step $(\triangle \phi)$ depends on the centre-to-centre spacing of adjacent cells, the frequency of operation and the

desired tilt angle. The required phase shift between two unit cells can be written as

$$\triangle \phi = \frac{2\pi d \sin \gamma}{\lambda_0} \tag{6.4}$$

where d is the centre-to-centre spacing between two unit cells, λ_0 is the free-space wavelength, and γ is the steering angle.

An ideal phase mapping of a BSM operating at 20 GHz is designed to tilt the beam at a 20° angle as
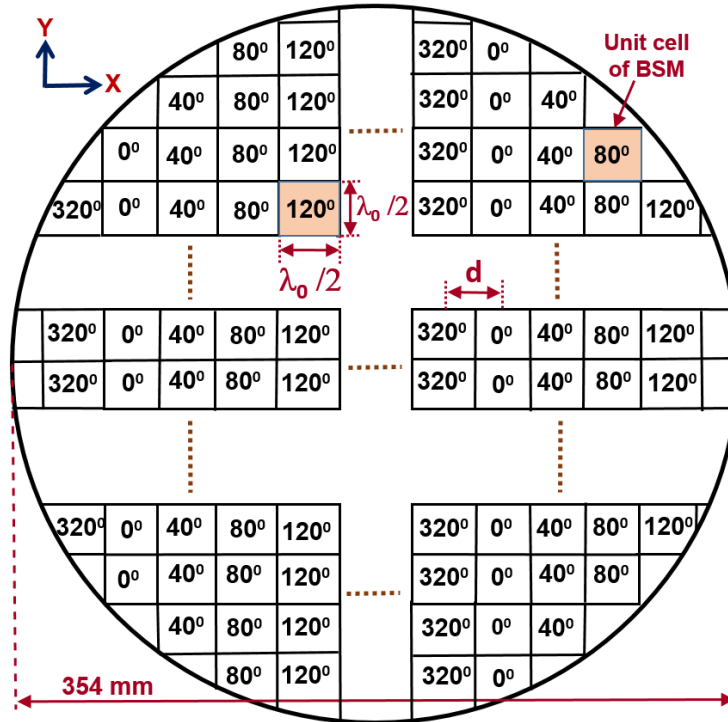
Figure 6.3: Sawtooth phase-shifting strategy to move the beam direction to an offset angle.

given in Figure 6.3. As can be seen from the figure, the phase increases on the surface of the BSM along the X-axis. As the phase repeats after a cycle of 360°, the phase shift is wrapped on the surface to make a sawtooth phase distribution. The phase shift of the BSM is realised using a metamaterial configuration similar to that discussed in [41].

The metasurface used here has four metallic layers and additionally has holes to increase the transmission phase range. Each metallic layers has square conducting patches and is separated by uniform dielectric layers as shown in Figure 6.4. The dielectric layers are composed of Taconic TLY-5 with the relative permittivity of 2.2 and loss tangent of 0.0009. Each dielectric layer has a thickness of 1.575 mm. The first and third metallic conducting patches have identical sizes represented by "a", and the second and fourth metallic patches have identical sizes represented by "b" as shown in Figure 6.4. The phase shift depends on the dimensions of the metallic patches "a" and "b". To get a particular
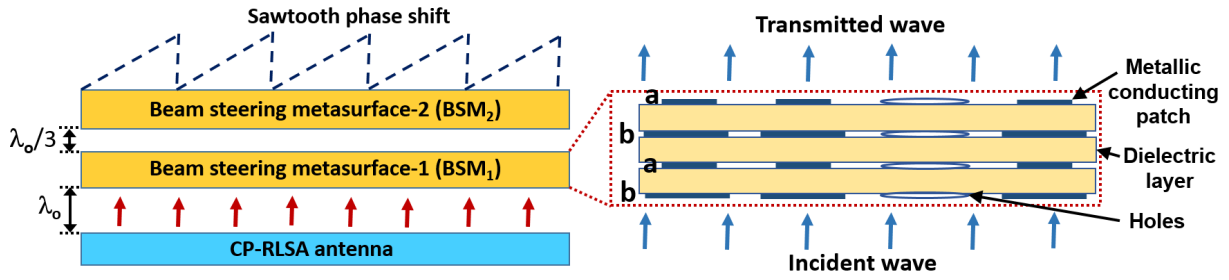
Figure 6.4: The cross-sectional view of RLSA antenna with beam-steering metasurfaces. "a" and "b" represent the sizes of the metallic conducting patches.

phase shift these dimensions were swept from 0.1 to 7.5 mm. Using this methodology both BSMs have been designed and simulated with a CP-RLSA antenna. The numerical results are discussed in the following section.

6.4 Numerical Results and Discussion

The 3D model of the antenna system with beam-steering metasurface is shown in Figure 6.5. It has only one BSM placed $1\lambda_\circ$ (15 mm) above the top surface of the CP-RLSA antenna. The BSM creates
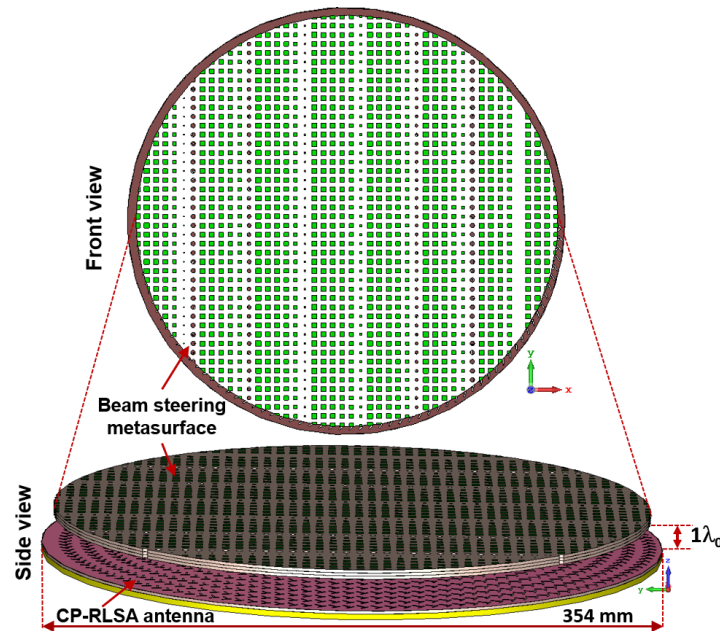
Figure 6.5: The 3D view of a beam-steering metasurface (BSM) with CP-RLSA antenna. The BSM is placed $1\lambda_\circ$ (15 mm) above the CP-RLSA antenna.

a sawtooth phase shift along the X-axis. Therefore, the antenna beam was steered at $\phi = 0°$ and $\theta = 20°$. The directivity and gain of the antenna, with the BSM positioned at ($\phi = \beta = 0°$), is shown in Figure 6.6. The peak directivity of 31 dBi was achieved with a peak gain of 30.4 dBic at 20.1 GHz. The axial ratio was taken in the direction of the main beam, which is $\theta = 20°$ and $\phi = 0°$, is also shown in Figure 6.6. The axial ratio is below the 3-dB level, which satisfies the circular polarisation requirement.

The BSM was rotated around the antenna axis (Z-axis) with 90° steps. Figure 6.7 shows the far-field radiation patterns at four different orientations of the BSM, $\beta = 0°, 90°, 180°,$ and $270°$ at 20 GHz. Each measured pattern has a beam tilt of $\theta = 20°$ in the elevation plane for each orientation of the
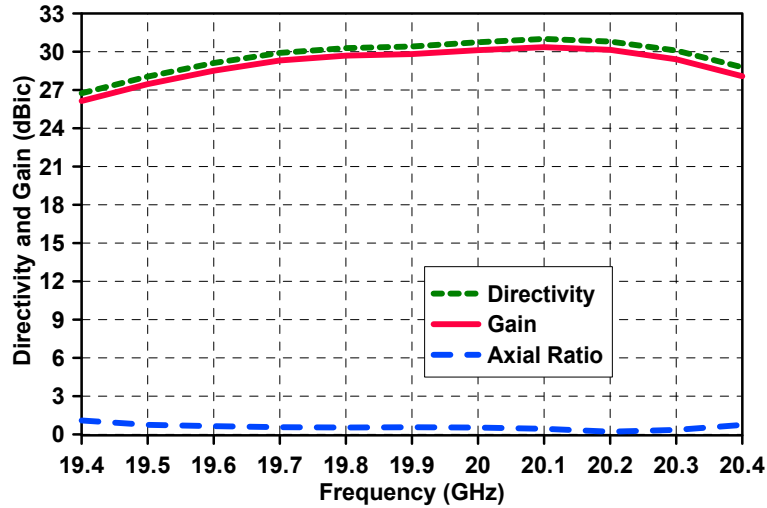
Figure 6.6: Peak directivity, gain and axial ratio of the CP-RLSA antenna with one BSM.
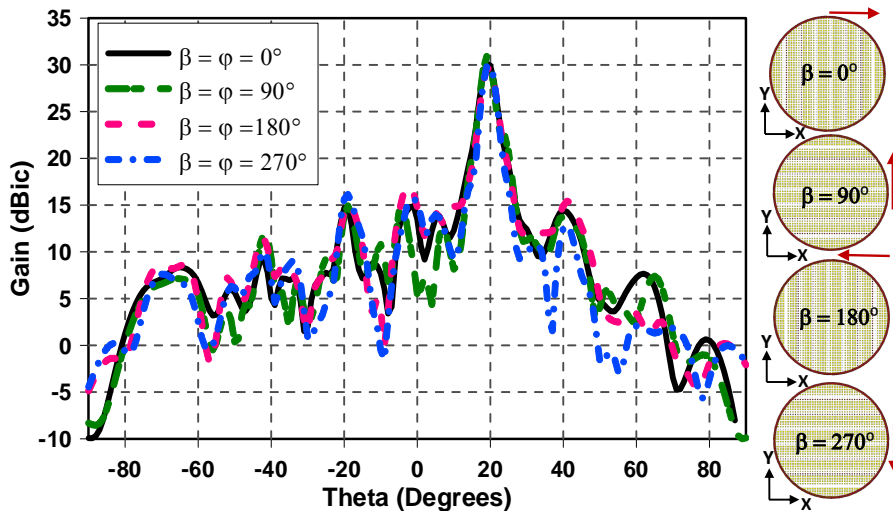
Figure 6.7: Far-field radiation patterns for four different orientations of BSM.

Table 6.1: Pattern quality for four different orientations of BSM at 20 GHz.

| Orientation of BSM	Steered beam direction		Peak gain	SLL	Total efficiency
(β) (deg.)	ϕ (deg.)	θ (deg.)	dBic	dB	%
0	0	20	30.1	-15.2	86.6
90	90	20	30.9	-16	86.7
180	180	20	29.6	-12.6	86.7
270	270	20	30	-14	87

BSM. The azimuth angle (ϕ) of the antenna beam follows the orientation of the BSM, hence the radiation beam moves on the surface of a cone. The reflection coefficients are less than -10 dB, and more than 90% radiation efficiencies are obtained with each antenna simulation.

The total antenna efficiency, and the pattern quality in terms of the gain and sidelobe level (SLL) at 20 GHz are summarised in Table 6.1. The highest gain of 30.9 dBic was achieved when the orientation of the BSM was along the Y-axis ($\beta = 90°$) and the lowest sidelobe level (-16 dB) was also obtained utilising the same orientation. As can be seen from the table, the SLLs are less than -12 dB, which indicates that the steered beams have good pattern qualities with an acceptable level. The quality of the pattern can be further improved by optimisation of the steering surface. This includes linearly increasing the sawtooth phase shift, which will reduce the reflections from the input side of the antenna and steering surface, and therefore will provide the highest transmission and higher gain.

Figure 6.8 shows the antenna with two BSMs which control the radiation beam direction in both the
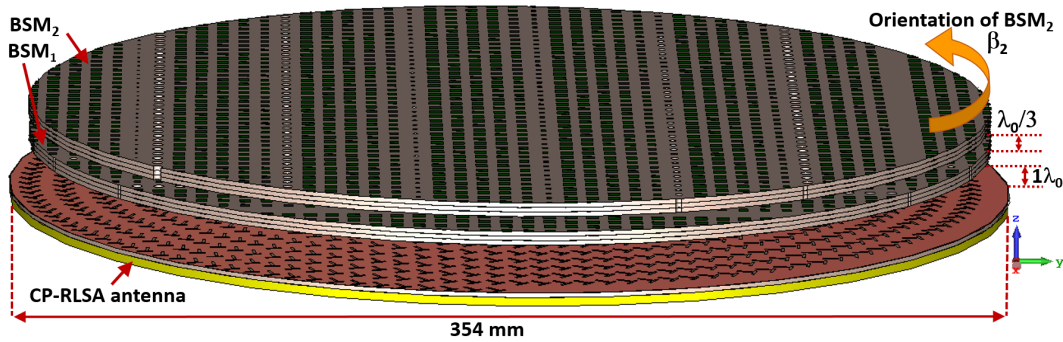

Figure 6.8: CST perspective view of a CP-RLSA antenna with two beam steering metasurfaces (BSM$_1$ & BSM$_2$). The orientation of BSM$_1$ is constant, while BSM$_2$ is rotated with an orientation angle of β_2.
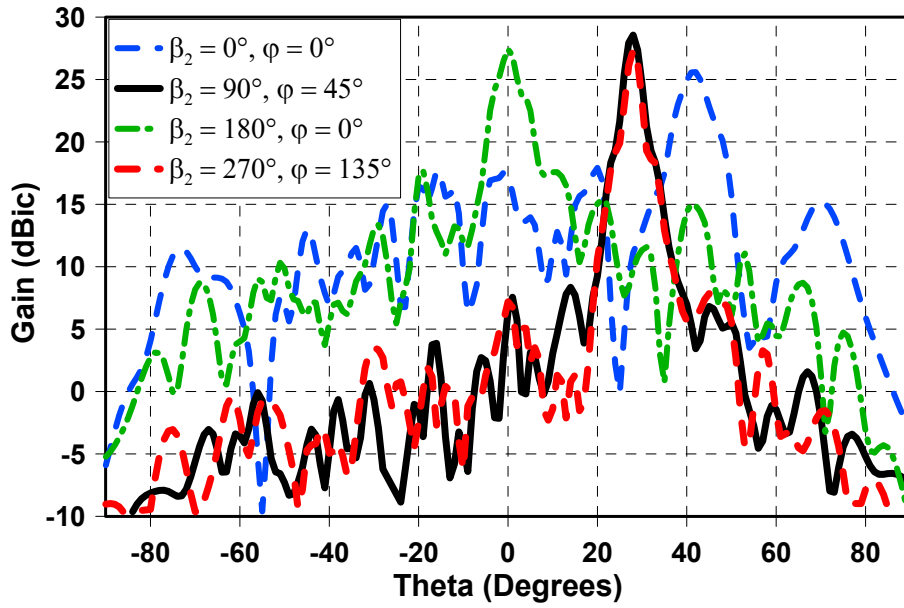
Figure 6.9: Far-field radiation patterns for four different orientations of BSM_2.

elevation and azimuth planes. Both BSMs are identical. BSM_1 is positioned $1\lambda_\circ$ (15 mm) above the CP-RLSA and the spacing between BSM_1 and BSM_2 is $\lambda_\circ/3$ (5 mm). The sawtooth orientation angle of BSM_1 was kept constant ($\beta_1 = 0°$), while β_2 of BSM_2 was turned in steps of $90°$, i.e. $\beta_2 = 0°$, $90°$, $180°$, $270°$. The far-field radiation patterns for each orientation are shown in Figure 6.9. The radiation cut patterns are taken at the elevation plane containing the peak beam direction.

The steered beam direction, peak gain, sidelobe level (SLL), and total antenna efficiency are summarised in Table 6.2. The highest peak gain of 28.6 dBic and the lowest sidelobe level of -20.2 dB are obtained with $90°$ orientation of BSM_2 and the beam points at $\theta = 28°$ and $\phi = 45°$. The gain drops and the beam gradually widens as the elevation angle increases. The lowest gain of 25.6 dBic occurs when the beam position is farthest from the broadside direction, i.e. $\theta = 42°$. The beam can be

Table 6.2: Pattern quality for four BSM_2 orientations at 20 GHz.

Orientation of BSM_1 & BSM_2		Steered beam direction		Peak gain	SLL	Efficiency
(β_1) (deg.)	(β_2) (deg.)	ϕ (deg.)	θ (deg.)	dBic	dB	%
0	0	0	42	25.6	-7.7	81
0	90	45	28	28.6	-20.2	80
0	180	0	0	27.4	-9.7	79
0	270	135	28	27.4	-19.5	80

moved in both the azimuth and elevation planes by co-rotating the two BSMs, enabling them to cover a conical region with a vertex angle of $84°(2 \times 42°)$.

6.5   Summary

A beam-steering method for RLSA antennas has been presented in this chapter. Two beam-steering metasurfaces were used to steer the beam direction of the antenna in both the azimuth and elevation planes by rotating the metasurface pair independently and together. High gain and good pattern qualities were achieved with the steered beams. The antenna maintains its planar geometry while steering the radiation beam in different directions. This assists in overcoming the limitations associated with the conventional mechanical beam-steering technique. This steering method does not have RF (radio frequency) components or multi-axis rotary joints because all the radiating elements are stationary. There are no biasing requirements, intermodulation distortion, heating problems, or RF losses. The antenna efficiencies were measured as high due to the lack of RF absorber. Since the antenna configuration is significantly simpler than the traditional beam-steered antennas, the fabrication cost can be less and installation can be simplified significantly.

Chapter 7

Conclusions and Future Work

7.1 Conclusions

RLSA antennas have shown the potential to serve as an alternative to traditional high-gain antennas due to their promising performance. They provide a very low-profile characteristic, planar configuration, simple feed transition, and highly directive radiation patterns. RLSA antennas are being viewed as the emerging candidate in several wireless communication applications. However, they provide narrowband behaviour and lack beam steering. Nonetheless, these antennas are highly desirable to meet suitable gain and compatible radiation pattern envelope (RPE) values for commercial deployment. In this thesis, we present the design methodology for wideband, beam-steered RLSA antennas and investigate if their pattern qualities are consistent with RPEs of Class-2 and Class-3 antennas, as specified by ETSI.

In the first step, a single-layer circularly polarised RLSA antenna was designed. The design methodology has simplified the design complexity of traditional RLSA antennas. The antenna has achieved a gain of 36.9 dBic with 62.7% aperture efficiency and 95% total efficiency. The antenna has demonstrated a very good return loss bandwidth (23.3%) and axial ratio over the frequency band of interest. Following this, we have analysed the field distribution of RLSA antennas and optimised their electric near field to improve the pattern quality. Two CP-RLSA antennas were designed, one with a tapered amplitude distribution and another with a uniform amplitude distribution. The distributions were obtained by controlling the slot coupling over the antenna aperture. The uniform amplitude distribution provided a better gain and 3-dB gain bandwidth, whereas the tapered amplitude distribution indicated a very good pattern quality, with controlled sidelobe level as low as -26.1 dB.

In the next step, we propose a new cavity configuration of RLSA antennas to enhance their limited

radiation bandwidth. The cavity was designed using radial permittivity variation of the dielectric materials. Some RLSA antenna prototypes were designed with the modified cavity and compared with the traditional RLSA antennas. An antenna has demonstrated 32 dBic gain with a 3-dB gain bandwidth of 19.4%. The antenna has successfully met the requirements of ETSI Class-2 and Class-3 antennas' RPE values.

Finally, we present a beam-steering RLSA antenna design method. The radiation beam was steered using near-field phase transformation. A pair of beam-steering metasurfaces (BSM) was used to shift the phase of an RLSA antenna in a linearly increasing phase to change the radiation beam direction from broadside to an offset angle. The radiation beam can be steered to the desired direction by co-rotation of the BSM pair. The beam moves within a large conical region without deteriorating the gain to a great extent. The beam steering method provides a number of advantages and overcomes the difficulties associated with traditional beam steering methods.

7.2 Future Work

This research work reveals scope for further investigation of RLSA antennas. The possibilities are as follows:

- The initial work carried out on the optimisation of the near-field distribution of RLSA antennas can be extended to achieve beam shaping.

- The pattern quality of the RLSA antennas with STPG-loaded cavity can be further improved by using a tapered amplitude distribution.

- The work on beam steering indicates that the gain and pattern quality of the antenna degrade when the beam moves further from the broadside. The gain and quality of the pattern can be improved by simplifying and optimising the metasurface design.

- As discussed in Chapter 6, the beam-steering metasurfaces are rotated around the antenna axis. For this reason, it is essential to have a rotationally symmetric field distribution from the feed antenna. For RLSA antennas, the symmetric field distribution can be improved by using concentric annular rings instead of spiral rings.

Appendix A

List of Acronyms

RLSA   Radial Line Slot Array

CP-RLSA   Circularly Polarised Radial Line Slot Array

LP-RLSA   Linearly Polarised Radial Line Slot Array

RPE   Radiation Pattern Envelope

TEM   Transverse Electromagnetic

SLL   Side Lobe Level

BSM   Beam Steering Metasurface

STPG   Substrate Transverse Permittivity Gradient

CST   Computer Simulation Technology

COTM   Communication On The Move

WLAN   Wireless Local Area Network

VBA   Visual Basic Macro

ETSI   European Telecommunications Standards Institute

HPM   High Power Microwave

DBS   Direct Broadcast Satellite

HFSS   High Frequency Structural Simulator

RCA   Resonant Cavity Antenna

MoM   Method of Moments

CW   Clockwise

CCW   Counter Clockwise

RF   Radio Frequency

Appendix B

Visual Basic Macros

Macros for generating slot layout with uniform amplitude distribution.

```vb
Sub Main ()
Static counter As Integer
Dim sCommand As String
Dim Sp As Double
Dim b As Double
Dim Current_spacing As Double
Dim ring As Integer
Dim Slot_no As Integer
Dim Angular_spacing As Double
Dim Current_theta As Double
Dim rounded_slot As Integer
Dim theta As Double
Dim slot_length As Double
Dim slot_width As Double
Dim slot_depth As Double
Dim Rho_s As Double
Dim Rho_phi As Double
Dim first_radius As Double
Dim no_of_rings As Integer
Dim i As Integer
Dim j As Integer
Dim theta1 As Double
Dim radius1 As Double
counter=0
slot_width=1
slot_depth=.035
```

```
27  no_of_rings=15
28  first_radius=15
29  Rho_s=12
30  b=Rho_s/(2*pi)
31  Rho_phi=7.5
32  For i=1 To no_of_rings
33      radius =first_radius + Rho_s*(i-1)
34      Slot_no= Round((2*pi*radius)/Rho_phi)
35      Angular_spacing = 2*pi/Slot_no
36      rounded_slot = Round(Slot_no)
37  For j=1 To rounded_slot
38      Current_theta = (2*pi*(i-1))+Angular_spacing*(j-1)
39      R=first_radius+b*Current_theta
40      theta=Current_theta
41      slot_length=4+(R*.008)
42      radius1=R+(Rho_s/4)
43      a3=.707*(Rho_s/4)
44      theta1=Atn(a3/radius1)
45      R2=a3/Sin(theta1)
46    x=R*Cos(theta)
47    y=R*Sin(theta)
48    x1=R2*Cos(theta+theta1)
49    y1=R2*Sin(theta+theta1)
50      counter=counter+1
51  'Create Brick
52  sCommand = ""
53  sCommand = sCommand+  "With Brick" + vbLf
54  sCommand = sCommand+     ".Reset" + vbLf
55  sCommand = sCommand +     ".Name " +Cstr(i)+Cstr(counter) + vbLf
56  sCommand = sCommand +     ".Component ""component1""" + vbLf
57  sCommand = sCommand +     ".Material ""Vacuum""" + vbLf
58  sCommand = sCommand +     ".Xrange "+ Cstr(x-slot_length/2)+","+Cstr(x+
        slot_length/2) + vbLf
59  sCommand = sCommand +    ".Yrange "+ Cstr(y-slot_width/2)+","+Cstr(y+slot_width
        /2) + vbLf
60  sCommand = sCommand +    ".Zrange ""0""," + Cstr(slot_depth) + vbLf
61  sCommand = sCommand +     ".Create" + vbLf
62  sCommand = sCommand+ "End With" + vbLf
63  AddToHistory "Transform: component1_Slot"+Cstr(counter), sCommand
```

```
64  ' Rotate Brick
65  sCommand = ""
66  sCommand = sCommand + "" + vbLf
67  sCommand=sCommand+   "With Transform" +vbLf
68  sCommand=sCommand+        ".Reset" +vbLf
69  sCommand=sCommand+        ".Name ""component1:""& "+Cstr(i)+Cstr(counter)  +vbLf
70  sCommand=sCommand+        ".Origin ""CommonCenter"" "   +vbLf
71  sCommand=sCommand+        ".Center ""0"", ""0"", ""0"" " +vbLf
72  sCommand=sCommand+        ".Angle ""0"", ""0"" ," + Cstr(((theta)*180/pi)) + vbLf
73  sCommand=sCommand+        ".MultipleObjects ""False"" "   +vbLf
74  sCommand=sCommand+        ".GroupObjects ""False"" " +vbLf
75  sCommand=sCommand+        ".Repetitions ""1"" "   +vbLf
76  sCommand=sCommand+        ".MultipleSelection ""False""" +vbLf
77  sCommand=sCommand+        ".Destination ""component1"" " +vbLf
78  sCommand=sCommand+        ".Material """" "   +vbLf
79  sCommand=sCommand+        ".Transform ""Shape"", ""Rotate"" "  +vbLf
80  sCommand=sCommand+ "End With"
81  AddToHistory "Transform: component1_rotate"+Cstr(counter), sCommand
82  ' Rotate Brick
83  sCommand = ""
84  sCommand = sCommand + "" + vbLf
85  sCommand=sCommand+   "With Transform" +vbLf
86  sCommand=sCommand+        ".Reset" +vbLf
87  sCommand=sCommand+        ".Name ""component1:""& "+Cstr(i)+Cstr(counter)  +vbLf
88  sCommand=sCommand+        ".Origin ""CommonCenter"" "   +vbLf
89  sCommand=sCommand+        ".Center ""0"", ""0"", ""0"" " +vbLf
90  sCommand=sCommand+        ".Angle ""0"", ""0"" ," + Cstr((pi/4)*180/pi)   + vbLf
91  sCommand=sCommand+        ".MultipleObjects ""False"" "   +vbLf
92  sCommand=sCommand+        ".GroupObjects ""False"" " +vbLf
93  sCommand=sCommand+        ".Repetitions ""1"" "   +vbLf
94  sCommand=sCommand+        ".MultipleSelection ""False""" +vbLf
95  sCommand=sCommand+        ".Transform ""Shape"", ""Rotate"" "  +vbLf
96  sCommand=sCommand+ "End With"
97  AddToHistory "Transform: component1_rotate"+Cstr(counter), sCommand
98  'Create Brick pair
99  sCommand = ""
100 sCommand = sCommand+  "With Brick" + vbLf
101 sCommand = sCommand+     ".Reset" + vbLf
102 sCommand = sCommand +     ".Name " +Cstr(i)+Cstr(counter) + vbLf
```

```vb
103  sCommand = sCommand +      ".Component ""component2"""  + vbLf
104  sCommand = sCommand +      ".Material ""Vacuum"""  + vbLf
105  sCommand = sCommand +      ".Xrange "+ Cstr(x1-slot_length/2)+","+Cstr(x1+
         slot_length/2) + vbLf
106  sCommand = sCommand +    ".Yrange "+ Cstr(y1-slot_width/2)+","+Cstr(y1+slot_width
         /2) + vbLf
107  sCommand = sCommand +      ".Zrange ""0""," + Cstr(slot_depth) + vbLf
108  sCommand = sCommand +      ".Create" + vbLf
109  sCommand = sCommand+ "End With" + vbLf
110  AddToHistory "Transform: component2_Slot"+Cstr(counter), sCommand
111  ' Rotate Brick
112  sCommand = ""
113  sCommand = sCommand + "" + vbLf
114  sCommand=sCommand+   "With Transform" +vbLf
115  sCommand=sCommand+        ".Reset" +vbLf
116  sCommand=sCommand+        ".Name ""component2:""& "+Cstr(i)+Cstr(counter)   +vbLf
117  sCommand=sCommand+        ".Origin ""CommonCenter"" "   +vbLf
118  sCommand=sCommand+        ".Center ""0"", ""0"", ""0"" " +vbLf
119  sCommand=sCommand+        ".Angle ""0"", ""0"" ," + Cstr(((theta)*180/pi)) + vbLf
120  sCommand=sCommand+        ".MultipleObjects ""False"" "   +vbLf
121  sCommand=sCommand+        ".GroupObjects ""False"" " +vbLf
122  sCommand=sCommand+        ".Repetitions ""1"" "   +vbLf
123  sCommand=sCommand+        ".MultipleSelection ""False""" +vbLf
124  sCommand=sCommand+        ".Destination ""component2"" " +vbLf
125  sCommand=sCommand+        ".Material """ "   +vbLf
126  sCommand=sCommand+        ".Transform ""Shape"", ""Rotate"" "   +vbLf
127  sCommand=sCommand+ "End With"
128  AddToHistory "Transform: component2_rotate"+Cstr(counter), sCommand
129  ' Rotate Brick
130  sCommand = ""
131  sCommand = sCommand + "" + vbLf
132  sCommand=sCommand+   "With Transform" +vbLf
133  sCommand=sCommand+        ".Reset" +vbLf
134  sCommand=sCommand+        ".Name ""component2:""& "+Cstr(i)+Cstr(counter)   +vbLf
135  sCommand=sCommand+        ".Origin ""CommonCenter"" "   +vbLf
136  sCommand=sCommand+        ".Center ""0"", ""0"", ""0"" " +vbLf
137  sCommand=sCommand+        ".Angle ""0"", ""0"" ," + Cstr(((pi/2)+(pi/4))*180/pi) +
         vbLf
138  sCommand=sCommand+        ".MultipleObjects ""False"" "   +vbLf
```

```
139  sCommand=sCommand+        ".GroupObjects ""False"" " +vbLf
140  sCommand=sCommand+        ".Repetitions ""1"" "   +vbLf
141  sCommand=sCommand+        ".MultipleSelection ""False""" +vbLf
142  sCommand=sCommand+        ".Transform ""Shape"", ""Rotate"" "   +vbLf
143  sCommand=sCommand+ "End With"
144  AddToHistory "Transform: component2_rotate"+Cstr(counter), sCommand
145  Next j
146  Next i
147  End Sub
```

Macros for generating slot layout with tapered amplitude distribution.

```
1   Sub Main ()
2   Static counter As Integer
3   Dim sCommand As String
4   Dim Sp As Double
5   Dim b As Double
6   Dim Current_spacing As Double
7   Dim ring As Integer
8   Dim Slot_no As Integer
9   Dim Angular_spacing As Double
10  Dim Current_theta As Double
11  Dim rounded_slot As Integer
12  Dim theta As Double
13  Dim slot_length As Double
14  Dim slot_width As Double
15  Dim slot_depth As Double
16  Dim Rho_s As Double
17  Dim Rho_phi As Double
18  Dim first_radius As Double
19  Dim no_of_rings As Integer
20  Dim i As Integer
21  Dim j As Integer
22  Dim theta1 As Double
23  Dim radius1 As Double
24  counter=0
25  slot_width=1
26  slot_depth=.035
27  no_of_rings=15
28  first_radius=15
```

```
29  Rho_s=12
30  b=Rho_s/(2*pi)
31  Rho_phi=7.5
32  For i=1 To no_of_rings
33      radius =first_radius + Rho_s*(i-1)
34      Slot_no= Round((2*pi*radius)/Rho_phi)
35      Angular_spacing = 2*pi/Slot_no
36      rounded_slot = Round(Slot_no)
37    For j=1 To rounded_slot
38      Current_theta = (2*pi*(i-1))+Angular_spacing*(j-1)
39      R=first_radius+b*Current_theta
40      theta=Current_theta
41      slot_length=4.8+(R*.004)
42      radius1=R+(Rho_s/4)
43      a3=.707*(Rho_s/4)
44      theta1=Atn(a3/radius1)
45      R2=a3/Sin(theta1)
46    x=R*Cos(theta)
47    y=R*Sin(theta)
48    x1=R2*Cos(theta+theta1)
49    y1=R2*Sin(theta+theta1)
50      counter=counter+1
51  'Create Brick
52  sCommand = ""
53  sCommand = sCommand+  "With Brick" + vbLf
54  sCommand = sCommand+      ".Reset" + vbLf
55  sCommand = sCommand +     ".Name " +Cstr(i)+Cstr(counter) + vbLf
56  sCommand = sCommand +     ".Component ""component1""" + vbLf
57  sCommand = sCommand +     ".Material ""Vacuum""" + vbLf
58  sCommand = sCommand +     ".Xrange "+ Cstr(x-slot_length/2)+","+Cstr(x+
        slot_length/2) + vbLf
59  sCommand = sCommand +     ".Yrange "+ Cstr(y-slot_width/2)+","+Cstr(y+slot_width
        /2) + vbLf
60  sCommand = sCommand +     ".Zrange ""0""," + Cstr(slot_depth) + vbLf
61  sCommand = sCommand +     ".Create" + vbLf
62  sCommand = sCommand+ "End With" + vbLf
63  AddToHistory "Transform: component1_Slot"+Cstr(counter), sCommand
64  ' Rotate Brick
65  sCommand = ""
```

```vb
66 sCommand = sCommand + "" + vbLf
67 sCommand=sCommand+    "With Transform" +vbLf
68 sCommand=sCommand+        ".Reset" +vbLf
69 sCommand=sCommand+        ".Name ""component1:""& "+Cstr(i)+Cstr(counter)  +vbLf
70 sCommand=sCommand+        ".Origin ""CommonCenter"" "  +vbLf
71 sCommand=sCommand+        ".Center ""0"", ""0"", ""0"" " +vbLf
72 sCommand=sCommand+        ".Angle ""0"", ""0"" ," + Cstr(((theta)*180/pi)) + vbLf
73 sCommand=sCommand+        ".MultipleObjects ""False"" "  +vbLf
74 sCommand=sCommand+        ".GroupObjects ""False"" " +vbLf
75 sCommand=sCommand+        ".Repetitions ""1"" "  +vbLf
76 sCommand=sCommand+        ".MultipleSelection ""False""" +vbLf
77 sCommand=sCommand+        ".Destination ""component1"" " +vbLf
78 sCommand=sCommand+        ".Material """" "  +vbLf
79 sCommand=sCommand+        ".Transform ""Shape"", ""Rotate"" "  +vbLf
80 sCommand=sCommand+ "End With"
81 AddToHistory "Transform: component1_rotate"+Cstr(counter), sCommand
82 ' Rotate Brick
83 sCommand = ""
84 sCommand = sCommand + "" + vbLf
85 sCommand=sCommand+    "With Transform" +vbLf
86 sCommand=sCommand+        ".Reset" +vbLf
87 sCommand=sCommand+        ".Name ""component1:""& "+Cstr(i)+Cstr(counter)  +vbLf
88 sCommand=sCommand+        ".Origin ""CommonCenter"" "  +vbLf
89 sCommand=sCommand+        ".Center ""0"", ""0"", ""0"" " +vbLf
90 sCommand=sCommand+        ".Angle ""0"", ""0"" ," + Cstr((pi/4)*180/pi)  + vbLf
91 sCommand=sCommand+        ".MultipleObjects ""False"" "  +vbLf
92 sCommand=sCommand+        ".GroupObjects ""False"" " +vbLf
93 sCommand=sCommand+        ".Repetitions ""1"" "  +vbLf
94 sCommand=sCommand+        ".MultipleSelection ""False""" +vbLf
95 sCommand=sCommand+        ".Transform ""Shape"", ""Rotate"" "  +vbLf
96 sCommand=sCommand+ "End With"
97 AddToHistory "Transform: component1_rotate"+Cstr(counter), sCommand
98 'Create Brick pair
99 sCommand = ""
100 sCommand = sCommand+   "With Brick" + vbLf
101 sCommand = sCommand+       ".Reset" + vbLf
102 sCommand = sCommand +     ".Name " +Cstr(i)+Cstr(counter) + vbLf
103 sCommand = sCommand +     ".Component ""component2""" + vbLf
104 sCommand = sCommand +     ".Material ""Vacuum""" + vbLf
```

```
105  sCommand = sCommand +       ".Xrange "+ Cstr(x1-slot_length/2)+","+Cstr(x1+
         slot_length/2) + vbLf
106  sCommand = sCommand +       ".Yrange "+ Cstr(y1-slot_width/2)+","+Cstr(y1+slot_width
         /2) + vbLf
107  sCommand = sCommand +       ".Zrange ""0""," + Cstr(slot_depth) + vbLf
108  sCommand = sCommand +       ".Create" + vbLf
109  sCommand = sCommand+ "End With" + vbLf
110  AddToHistory "Transform: component2_Slot"+Cstr(counter), sCommand
111  ' Rotate Brick
112  sCommand = ""
113  sCommand = sCommand + "" + vbLf
114  sCommand=sCommand+   "With Transform" +vbLf
115  sCommand=sCommand+       ".Reset" +vbLf
116  sCommand=sCommand+       ".Name ""component2:""& "+Cstr(i)+Cstr(counter)   +vbLf
117  sCommand=sCommand+       ".Origin ""CommonCenter"" "   +vbLf
118  sCommand=sCommand+       ".Center ""0"", ""0"", ""0"" " +vbLf
119  sCommand=sCommand+       ".Angle ""0"", ""0"" ," + Cstr(((theta)*180/pi)) + vbLf
120  sCommand=sCommand+       ".MultipleObjects ""False"" "   +vbLf
121  sCommand=sCommand+       ".GroupObjects ""False"" " +vbLf
122  sCommand=sCommand+       ".Repetitions ""1"" "   +vbLf
123  sCommand=sCommand+       ".MultipleSelection ""False""" +vbLf
124  sCommand=sCommand+       ".Destination ""component2"" " +vbLf
125  sCommand=sCommand+       ".Material """" "   +vbLf
126  sCommand=sCommand+       ".Transform ""Shape"", ""Rotate"" "   +vbLf
127  sCommand=sCommand+ "End With"
128  AddToHistory "Transform: component2_rotate"+Cstr(counter), sCommand
129  ' Rotate Brick
130  sCommand = ""
131  sCommand = sCommand + "" + vbLf
132  sCommand=sCommand+   "With Transform" +vbLf
133  sCommand=sCommand+       ".Reset" +vbLf
134  sCommand=sCommand+       ".Name ""component2:""& "+Cstr(i)+Cstr(counter)   +vbLf
135  sCommand=sCommand+       ".Origin ""CommonCenter"" "   +vbLf
136  sCommand=sCommand+       ".Center ""0"", ""0"", ""0"" " +vbLf
137  sCommand=sCommand+       ".Angle ""0"", ""0"" ," + Cstr(((pi/2)+(pi/4))*180/pi) +
         vbLf
138  sCommand=sCommand+       ".MultipleObjects ""False"" "   +vbLf
139  sCommand=sCommand+       ".GroupObjects ""False"" " +vbLf
140  sCommand=sCommand+       ".Repetitions ""1"" "   +vbLf
```

```
141  sCommand=sCommand+        ".MultipleSelection ""False"""  +vbLf
142  sCommand=sCommand+        ".Transform ""Shape"", ""Rotate"" "   +vbLf
143  sCommand=sCommand+ "End With"
144  AddToHistory "Transform: component2_rotate"+Cstr(counter), sCommand
145  Next j
146  Next i
147  End Sub
```

References

[1] M. Sierra-Castaner, M. Sierra-Perez, M. Vera-Isasa, and J. L. Fernandez-Jambrina, "Low-cost monopulse radial line slot antenna," *IEEE Transactions on Antennas and Propagation*, vol. 51, no. 2, pp. 256–263, Feb 2003.

[2] C. W. Yuan, S. R. Peng, T. Shu, Z. Q. Li, and H. Wang, "Designs and experiments of a novel radial line slot antenna for high-power microwave application," *IEEE Transactions on Antennas and Propagation*, vol. 61, no. 10, pp. 4940–4946, Oct 2013.

[3] T. Nguyen, K. Sakurai, J. Hirokawa, M. Ando, O. Amano, S. Koreeda, T. Matsuzaki, and Y. Kamata, "A concise design of large mm-wave radial line slot antenna with honeycomb structures for space application," in *2014 XXXIth URSI General Assembly and Scientific Symposium (URSI GASS)*, Aug 2014, pp. 1–4.

[4] J. Suryana and D. B. Kusuma, "Design and implementation of RLSA antenna for mobile DBS application in Ku-band downlink direction," in *2015 International Conference on Electrical Engineering and Informatics (ICEEI)*, Aug 2015, pp. 341–345.

[5] M. Ando, K. Sakurai, N. Goto, K. Arimura, and Y. Ito, "A radial line slot antenna for 12 GHz satellite TV reception," *IEEE Transactions on Antennas and Propagation*, vol. 33, no. 12, pp. 1347–1353, Dec 1985.

[6] [Online]. Available: http://www-antenna.ee.titech.ac.jp/research/index-e.html

[7] K. Kelly, "Recent annular slot array experiments," in *1958 IRE International Convention Record*, vol. 5, March 1957, pp. 144–152.

[8] K. Kelly and F. Goebels, "Annular slot monopulse antenna arrays," *IEEE Transactions on Antennas and Propagation*, vol. 12, no. 4, pp. 391–403, Jul 1964.

[9]   M. Ando, K. Sakurai, and N. Goto, "Characteristics of a radial line slot antenna for 12 GHz band satellite TV reception," *IEEE Transactions on Antennas and Propagation*, vol. 34, no. 10, pp. 1269–1272, Oct 1986.

[10] M. Takahashi, J. I. Takada, M. Ando, and N. Goto, "A slot design for uniform aperture field distribution in single-layered radial line slot antennas," *IEEE Transactions on Antennas and Propagation*, vol. 39, no. 7, pp. 954–959, Jul 1991.

[11] M. Ando, T. Numata, J. I. Takada, and N. Goto, "A linearly polarized radial line slot antenna," *IEEE Transactions on Antennas and Propagation*, vol. 36, no. 12, pp. 1675–1680, Dec 1988.

[12] J. Takada, M. Ando, and N. Goto, "A reflection cancelling slot set in a linearly polarized radial line slot antenna," *IEEE Transactions on Antennas and Propagation*, vol. 40, no. 4, pp. 433–438, Apr 1992.

[13] M. Ando, "New DBS receiver antennas," in *1993 23rd European Microwave Conference*, Sept 1993, pp. 84–92.

[14] M. Takahashi, M. Ando, N. Goto, Y. Numano, M. Suzuki, Y. Okazaki, and T. Yoshimoto, "Dual circularly polarized radial line slot antennas," *IEEE Transactions on Antennas and Propagation*, vol. 43, no. 8, pp. 874–876, Aug 1995.

[15] P. W. Davis and M. E. Bialkowski, "Experimental investigations into a linearly polarized radial slot antenna for DBS TV in Australia," *IEEE Transactions on Antennas and Propagation*, vol. 45, no. 7, pp. 1123–1129, Jul 1997.

[16] P. W. Davis, "A linearly polarised radial line slot array antenna for direct broadcast satellite services," PhD dissertation, University of Queensland, Australia, 2000.

[17] P. W. Davis and M. E. Bialkowski, "Linearly polarized radial-line slot-array antennas with improved return-loss performance," *IEEE Antennas and Propagation Magazine*, vol. 41, no. 1, pp. 52–61, Feb 1999.

[18] M. E. Bialkowski and P. W. Davis, "Analysis of a circular patch antenna radiating in a parallel-plate radial guide," *IEEE Transactions on Antennas and Propagation*, vol. 50, no. 2, pp. 180–187, Feb 2002.

[19] S. Zagriatski and M. E. Bialkowski, "Circularly polarised radial line slot array antenna for wireless LAN access point," in *15th International Conference on Microwaves, Radar and Wireless Communications (IEEE Cat. No.04EX824)*, vol. 2, May 2004, pp. 649–652.

[20] K. Sudo, J. Hirokawa, and M. Ando, "Analysis of a slot pair coupling on a radial line filled with double-layer dielectric," in *2005 IEEE Antennas and Propagation Society International Symposium*, vol. 3A, July 2005, pp. 724–727.

[21] T. Lim and K. Tan, "The development of radial line slot array antenna for direct broadcast satellite reception," *International journal of electronics*, vol. 94, no. 3, pp. 251–261, 2007.

[22] M. Albani, A. Mazzinghi, and A. Freni, "Automatic design of CP-RLSA antennas," *IEEE Transactions on Antennas and Propagation*, vol. 60, no. 12, pp. 5538–5547, Dec 2012.

[23] S. Peng, C. W. Yuan, T. Shu, J. Ju, and Q. Zhang, "Design of a concentric array radial line slot antenna for high-power microwave application," *IEEE Transactions on Plasma Science*, vol. 43, no. 10, pp. 3527–3529, Oct 2015.

[24] S. I. Zakwoi, T. A. Rahman, I. Maina, and O. Elijah, "Design of Ka band downlink radial line slot array antenna for direct broadcast satellite services," in *2014 IEEE Asia-Pacific Conference on Applied Electromagnetics (APACE)*, Dec 2014, pp. 159–162.

[25] I. Maina, T. A. Rahman, and M. Khalily, "Bandwidth enhanced and sidelobes level reduced radial line slot array antenna at 28 GHz for 5G next generation mobile communication," *ARPN Journal of Engineering and Applied Sciences*, vol. 10, pp. 5752–5757, 2015.

[26] Y. Liu, H. Xiao, and G. Lu, "Design of a high gain circular polarized radial line slot antenna," in *2014 Seventh International Symposium on Computational Intelligence and Design*, vol. 2, Dec 2014, pp. 490–493.

[27] I. M. Ibrahim, T. A. Rahman, M. I. Sabran, and M. F. Jamlos, "Bandwidth enhancement through slot design on RLSA performance," in *2014 IEEE Region 10 Symposium*, April 2014, pp. 228–231.

[28] N. X. Tung, R. Jayawardene, Y. Takano, K. Sakurai, J. Hirokawa, M. Ando, O. Amano, T. Matsuzaki, S. Koreeda, T. Toda, Y. Kamata, K. Kawahara, Y. Tsuda, and M. Yoshikawa, "Characteristics of a high gain and light weight radial line slot antenna with honeycomb structure in

32GHz band for data link in space exploration," in *2012 International Symposium on Antennas and Propagation (ISAP)*, Oct 2012, pp. 154–157.

[29] T. X. Nguyen, R. S. Jayawardene, Y. Takano, K. Sakurai, T. Hirano, J. Hirokawa, M. Ando, O. Amano, S. Koreeda, and T. Matsuzaki, "Study of a high gain radial line slot antenna in Ka-band for space uses," in *2013 International Symposium on Electromagnetic Theory*, May 2013, pp. 611–613.

[30] T. Nguyen, J. Hirokawa, M. Ando, O. Amano, S. Koreeda, and T. Matsuzaki, "Material choices of honeycomb structures and their effects in mm-wave RLSAs," in *2014 IEEE Fifth International Conference on Communications and Electronics (ICCE)*, July 2014, pp. 417–419.

[31] Y. Wang, H. Xiao, G. Lu, J. Lin, and T. Li, "The investigation for a circularly polarized radial line slot antenna with low side lobes and high gain," in *2012 International Conference on Microwave and Millimeter Wave Technology (ICMMT)*, vol. 3, May 2012, pp. 1–2.

[32] M. Unno, J. Hirokawa, and M. Ando, "A double-layer dipole-array polarizer with a low-sidelobe radial line slot antenna," in *2007 Asia-Pacific Microwave Conference*, Dec 2007, pp. 1–4.

[33] J. I. Herranz-Herruzo, A. Valero-Nogueira, E. Alfonso, and V. M. Rodrigo, "Linearly-polarized radial-line slot-dipole array antenna without canceling elements," in *2007 IEEE Antennas and Propagation Society International Symposium*, June 2007, pp. 4296–4299.

[34] O. Beheshti-Zavareh and M. Hakkak, "A stable design of coaxial adaptor for radial line slot antenna," *Progress In Electromagnetics Research*, vol. 90, pp. 51–62, 2009.

[35] M. E. Bialkowski, "Analysis of a coaxial-to-waveguide adaptor including a descended probe and a tuning post," *IEEE Transactions on Microwave Theory and Techniques*, vol. 43, no. 2, pp. 344–349, Feb 1995.

[36] A. Mazzinghi, M. Albani, and A. Freni, "Double-spiral linearly polarized RLSA," *IEEE Transactions on Antennas and Propagation*, vol. 62, no. 9, pp. 4900–4903, Sept 2014.

[37] J. M. F. Gonzalez, P. Padilla, G. Exposito-Dominguez, and M. Sierra-Castaner, "Lightweight portable planar slot array antenna for satellite communications in X-Band," *IEEE Antennas and Wireless Propagation Letters*, vol. 10, pp. 1409–1412, 2011.

[38] C. A. Balanis, *Antenna theory: analysis and design*.   John Wiley & Sons, 2016.

[39] R. M. Hashmi and K. P. Esselle, "A class of extremely wideband resonant cavity antennas with large directivity-bandwidth products," *IEEE Transactions on Antennas and Propagation*, vol. 64, no. 2, pp. 830–835, Feb 2016.

[40] M. U. Afzal, "Near-field phase transformation for radiation performance enhancement and beam steering of resonant cavity antennas," PhD dissertation, Macquarie University, Australia, 2016.

[41] M. U. Afzal and K. P. Esselle, "Steering the beam of medium-to-high gain antennas using near-field phase transformation," *IEEE Transactions on Antennas and Propagation*, vol. 65, no. 4, pp. 1680–1690, April 2017.